

Field effect investigations of charge carrier transport in organic semiconductors

Von der Fakultät für Mathematik und Naturwissenschaften
der Carl von Ossietzky Universität Oldenburg
zur Erlangung des Grades und Titels eines
Doktors der Naturwissenschaften (Dr. rer. nat.)
angenommene Dissertation

von

Elizabeth von Hauff
geboren am 20.09.1977 in York, Kanada



Erstgutachter: Prof. Dr. Vladimir Dyakonov

Zweitgutachter: Prof. Dr. Jürgen Parisi and apl. Prof. Dr. Wilfried Tuszynski

Tag der Disputation: 19.12.2005

Abstract

Organic semiconductors are potentially a cost and energy effective alternative to conventional technologies. The understanding of charge transport in these materials and minimizing electrical losses in organic devices is essential to improve device output. In this thesis the transport properties of charge carriers in solution processed organic semiconductors were investigated via field effect measurements. Measurements of the temperature and electric field dependent charge carrier mobilities in organic field effect transistors (OFETs) is a good method for studying the transport properties in organic semiconductors.

In the first part of the thesis, the field effect characteristics of a methanofullerene [6,6]-phenyl C₆₁-butyric acid methyl ester (PCBM) OFET were modelled with a model from the literature for field effect theory in organic semiconductors. The results for the material parameters attained from the fit were compared to material parameters found in the literature from a study on fullerene diodes, with good agreement. Some discrepancy was then found between the current-voltage curves simulated with the material parameters and the experimentally determined data. This effect was attributed to contact resistances between the source and drain contacts and the PCBM layer. The contact resistances in OFETs have been observed to follow the same physics as the field effect mobility in low mobility materials; both depend on the injection conditions from metal into semiconductor. Values for the contact resistance were determined experimentally for various gate voltages at room temperature, and a general expression for the temperature and electric field dependence of the contact resistance was proposed. Accounting for the contact resistance led to a better agreement between the experimental and simulated values.

In the second part, the polymer-fullerene blends used in polymer photovoltaics were investigated. It is known that tempering is necessary

to enhance the performance of poly(3-hexylthiophene)(P3HT) based devices. The effect of tempering was investigated through changes in the field effect mobilities in the pure P3HT films and then in PCBM:P3HT blends. Tempering was found to result in a profound increase in the electron mobilities in the blends. The concentration of PCBM in the blend was then varied, to determine the optimal blend composition. Electron and hole mobilities were found to be balanced in the low $10^{-3}\text{cm}^2/\text{Vs}$ range for the 2:1 PCBM:P3HT blends. Charge carrier mobilities were consistently lower in the blends, suggesting that morphology is still an issue for charge transport.

Zusammenfassung

Organische Halbleiter haben das Potential ökonomischer in der Herstellung zu sein als herkömmliche anorganische Halbleiter. Grundlegendes Verständnis über Ladungstransporte im Material und die Minimierung elektrischer Verluste am Metall-Halbleiterübergang sind wichtig für die Optimierung der Leistung organischer Bauelemente. In dieser Arbeit wurden mit Hilfe von Feldeffekt-Messungen die Transporteigenschaften von organischen Halbleitern untersucht. Mobilitätsmessungen an organischen Feldeffekttransistoren (OFET) in Abhängigkeit der Temperatur und des elektrischen Feldes ist eine gute Methode die Transporteigenschaften organischer Halbleiter zu untersuchen.

Im ersten Teil dieser Arbeit wurden die Feldeffekt-Charakteristika eines Fulleren-OFETs mit einem aus der Literatur bekannten Model der Feldeffekttheorie für organische Halbleiter modelliert. Ein Vergleich der Materialparameter von dem angewandten Model mit gewonnenen Materialparametern einer Studie über Fulleren-Dioden aus der Literatur zeigte eine gute übereinstimmung der Werte. Mit diesen Materialparametern simulierte Strom-Spannungskurven wiesen Unterschiede zu gemessenen Daten auf, die den Kontaktwiderständen zwischen Metallkontakt und Halbleiter zugeschrieben wurden. Es wurde beobachtet, dass sich der Kontaktwiderstand physikalisch wie die Feldeffektbeweglichkeit in Materialien mit niedrigen Ladungsträgerbeweglichkeit beschreiben lässt; beide Größen hängen von den Injektionseigenschaften vom Kontaktmaterial in den Halbleiter ab. Der Kontaktwiderstand wurde bei Raumtemperatur für unterschiedliche Gate-Spannungen experimentell bestimmt, und eine allgemeine Beschreibung für die Abhängigkeit des Kontaktwiderstandes von der Temperatur und dem elektrischen Feld wurde vorgeschlagen. Die Beschreibung für den Kontaktwiderstand wurde in das Model eingebracht wodurch die Unterschiede zwischen simulierten und experimentellen Daten minimiert wurden.

Im zweiten Teil der Arbeit wurden die in der Polymerphotovoltaik verwandten Polymer-Fulleren-Mischungen untersucht. Es ist bekannt, dass das Tempern nötig ist, um die Leistung der auf poly(3-hexylthiophene)(P3HT) basierenden Bauelemente zu verbessern. Der Effekt des Temperns wurde sowohl an den reinen P3HT OFETs als auch an den PCBM:P3HT Mischungen untersucht. Das Tempern führt zu einer Erhöhung der Elektronenbeweglichkeit in den Mischungen. Die Konzentration des PCBMs in den Mischungen wurde variiert, um die optimale Zusammensetzung zu bestimmen. Für die 2:1 PCBM:P3HT Mischungen wurden gleiche Elektronen- und Lochbeweglichkeiten gefunden, die im unteren $10^{-3} \text{ cm}^2/\text{Vs}$ Bereich liegen. Ladungsträgerbeweglichkeiten waren in den Mischungen immer niedriger, was darauf hindeutet, dass die Morphologie ein wichtiger Punkt bei dem Ladungsträgertransport darstellt.

Contents

1	Organic semiconductors	1
1.1	Introduction	1
1.2	Electrical conduction in carbon based materials	2
1.3	Charge transport in organic semiconductors	4
2	Investigating charge transport in organic diodes	6
2.1	Organic light emitting diodes (OLEDs)	6
2.2	Space charge limited currents (SCLC)	7
2.2.1	Determining charge carrier mobilities from SCLC measurements	9
2.2.2	The SCLC Model in combination with other effects	9
2.2.2.1	Distribution of traps	10
2.2.2.2	Recombination	10
2.2.2.3	Built-in potential	10
2.3	Example of SCLC currents in polymer diodes	11
3	Charge carrier injection in organic semiconducting devices	13
3.1	Injection barrier heights	13
3.2	Injection models	14
3.3	Experimental studies of charge carrier injection into organic semiconductors	16
3.3.1	Investiations of the injection efficiency of a contact	16

3.3.2	Investigations of charge carrier injection via contact effects in organic field effect transistors	17
3.3.3	Bilayers for efficient charge injection	18
4	Charge transport in organic field effect transistors (OFETs)	19
4.1	Background	19
4.2	FET structures	20
4.2.1	Metal-Oxide-Semiconductor FETs (MOSFETs)	21
4.3	OFETs	24
4.3.1	Structure and current-voltage characteristics of OFETs	24
4.3.2	The field effect mobility	25
4.3.3	The Meyer-Neldel rule in OFETs	26
4.4	Modelling charge transport in OFETs	28
4.5	Contact effects in OFETs	29
4.6	Modelling charge transport in fullerene OFETs	31
4.6.1	Experimental	33
4.6.2	Room temperature field effect mobilities	33
4.6.3	Temperature dependent current-voltage characteristics	36
4.6.4	Material parameters: comparison with values in the literature	38
4.6.5	Temperature dependent field effect mobilities	39
4.6.6	Correction due to the effects of contact resistances	40
4.6.6.1	Modelling the temperature and field dependence of the contact resistance	40
4.6.6.2	Correction to the simulated current-voltage data	43
4.6.6.3	Correction to the simulated field effect mobility data	44
4.7	Summary	45

5 Organic photovoltaics: improving blend morphology in polymer-fullerene solar cells	47
5.1 Organic photovoltaics	47
5.1.1 History and development of organic solar cells	47
5.1.2 Feasibility of organic solar cells	50
5.2 Principals behind the polymer solar cell	50
5.2.1 The open-circuit voltage	52
5.2.2 The effect of morphology in polymer solar cells	53
5.3 Experimental	54
5.3.1 Field effect mobilities in P3HT films	55
5.3.1.1 Tempering in P3HT films	55
5.3.1.2 Consideration of contact effects	56
5.3.2 The effect of tempering in the polymer-fullerene blends	57
5.3.2.1 Variation of PCBM content in the blend	57
5.3.2.2 The effect of tempering on electron transport in blends	59
5.4 Summary	62
6 Conclusions	64
7 Appendix A: Experimental Setup	66
7.1 General	66
7.2 Samples	66
7.3 Sample holder	67
7.4 Current-voltage sweep	68
7.5 Temperature dependent measurements	69
Bibliography	70
Acknowledgements	83
Curriculum Vitae	84

Chapter 1

Organic semiconductors

1.1 Introduction

In recent years, there has been a lot of research done on organic semiconductors. Small molecule organic semiconductors were already being investigated over 60 years ago [1], however, the discovery of conducting polymers and the work done to improve their conductivity [2] offered to revolutionise electronics as these materials could be processed in solution form. The result is low cost and low energy device production, as well as the potential for large scale and flexible applications. Since then, studies have focused on explaining the charge transport properties within these materials, many device architectures have been investigated, including organic light emitting diodes (OLEDs), organic field effect transistors (OFETs), organic solar cells, polymer lasers, polymer batteries and polymer supercapacitors, and much work has been done towards improving device efficiencies.

In this thesis the charge transport properties of charge carriers in organic semiconductors are examined, specifically the transport properties in solution processable organic semiconducting materials. The thesis begins with the basic charge transport in an amorphous medium. In materials with such low charge carrier densities, injection conditions and the dynamics at the interface can be deciding for device performance. The interface between metal and semiconductor as well as general contact effects in organic devices are discussed and the spectrum of injection models is briefly presented. There have been many advances in OLED

1.2 Electrical conduction in carbon based materials

as well as in OFET technology, and these are reviewed. In addition, it is discussed how materials can be characterised in the diode or thin film transistor structure for screening purposes. The charge transport in fullerene OFETs is investigated, and the injection processes in these devices is studied. Organic photovoltaics, perhaps one of the most interesting fields in organic electronics from a social perspective, is the last topic that is dealt with. Advances in this field as well as the improvement of the active layer morphology and composition are discussed.

1.2 Electrical conduction in carbon based materials

Organic semiconductors are carbon based materials. The carbon atoms are joined by alternating single and double bonds, and the conjugated nature of the system leads to the semiconducting properties in these materials. In the carbon atom there are four electrons in the outer shell, which in the ground state are found in the $1s^2 2s^2 2p^2$ configuration. In organic semiconductors, there is a hybridization of the s and p orbitals to form 3 sp^2 orbitals. These orbitals are positioned 120° apart, forming a triangle coplanar to the carbon atoms. These orbitals form the stronger σ bonds. The fourth orbital is the p_z orbital, which is perpendicular to the plane of the atoms. The overlap of the p_z electrons from the carbon atoms form a delocalised band, the π orbitals, which are responsible for the conductive nature of the material [1].

The system may be expected to behave as a one dimensional metal, however, symmetry breaking reduces the energy of the system, resulting in two delocalised energy bands, the highest occupied molecular orbital (HOMO) and the lowest occupied molecular orbital (LUMO), separated by an energy gap. The one dimensional metal then becomes an insulator with a band gap in the order of one to a few electron volts. The value of the energy gap depends on the structure of the material [1; 3], and decreases for an increasing number of repeat units comprising the molecule [1; 3; 4]. The molecules are bound by strong covalent forces, the bonds between the molecules, however, are bound by weaker van der Waals forces. The properties in organic semiconductors are then determined by

1.2 Electrical conduction in carbon based materials

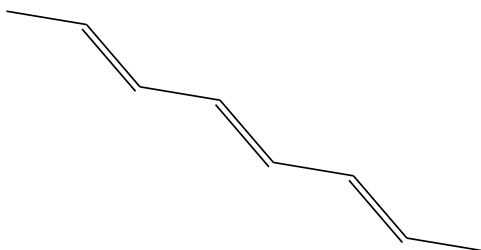


Figure 1.1: Example of a simple conjugated carbon chain

the more prominent molecular characteristics rather than those of the whole solid [1].

There is a large variety of organic semiconducting materials, and the possibilities for new materials is next to endless, as semiconductors can potentially be designed and synthesised according to the application. Organic semiconductors can be very roughly broken into two groups. The first group consists of the small molecule organic semiconductors which are deposited by means of vacuum deposition to form ordered films. Organic semiconductors of this form were already being investigated in the 1940's [1].

The discovery of conductive polymers in the late 70's [2], however, signified a breakthrough in electronics. A new group of materials was being investigated that could be processed in solution form. Electronic devices could be manufactured at low temperatures with minimal cost and energy expenditure. These materials lend themselves to large scale and flexible applications, for which conventional semiconductors are too expensive or too brittle. The discovery and continued work on conducting polymers led to the Nobel Prize in Chemistry in 2000 for Heeger, MacDiarmid and Shirakawa.

The solution processing of organic semiconductors can lead to higher disorder in the film and therefore lower mobilities compared to other deposition techniques such as vacuum deposition [5]. The difference in intra- and intermolecular charge carrier mobilities in the solution processed films illustrates this point. Charge

1.3 Charge transport in organic semiconductors

carrier mobilities on the individual molecules can be orders of magnitude larger than charge carrier mobilities through the films [6; 7; 8]. A higher degree of order in the semiconducting film can be attained through improved processing conditions and can lead to higher mobilities. For example, field effect mobilities in regioregular polythiophene in the order of $0.1\text{cm}^2/\text{Vs}$ have been reported for films in which tempering or self-organisation was used to improve polymer chain ordering [9; 10; 11]. One major focus point of the research in the area of organic electronics is the improvement of charge carrier transport through the semiconducting films for better device performance.

1.3 Charge transport in organic semiconductors

Due to the amorphous structure of organic semiconductors, energy sites within the materials are strongly localised. In materials governed by positional and energetic disorder, charge transport occurs via hopping [12; 13] between the localised sites.

Hopping transport in organic materials is commonly described by Miller-Abrahams formalism [14; 15]. The hopping rate is then given by

$$\nu_{ij} = \nu_o \exp(-2\gamma\Delta R_{ij}) \begin{cases} \exp(-\frac{E_j - E_i}{k_B T}); & E_j > E_i \\ 1; & E_j < E_i \end{cases} \quad (1.1)$$

where γ is the inverse localisation radius of the electronic wave function, ΔR_{ij} is the distance between localised sites i and j , and k_B is the Boltzmann constant.

The absorption bands of organic semiconductors are typically found to exhibit a Gaussian shape; charge transport in these materials is usually described with a Gaussian density of states (DOS) [15]:

$$g(E) = \frac{N}{\sqrt{2\pi}\sigma} \exp\left(-\frac{E^2}{2\sigma^2}\right) \quad (1.2)$$

where N is the number of energy sites per unit volume. The distribution is centered around zero energy, with a distribution width of σ .

The description of hopping transport in a disordered system introduced here can be simplified by employing the concept of a transport energy [16; 17; 18],

1.3 Charge transport in organic semiconductors

E_t , which reduces the problem of hopping transport in an amorphous medium to trap controlled band transport [19; 20]. Charge carriers in shallow energy sites ($E_i < E_t$) will hop to sites with lower energy ($E_i < E$) that are close by. For charge carriers at lower energy sites ($E_i > E_t$), the most probable hop upwards in energy is a hop to a site with $E \sim E_t$, regardless of the value of E_i . This means that hopping transport processes within the system revolve around E_t [21]. In organic semiconductors the transport energy plays the role of the mobility edge, which in inorganic non-crystalline semiconductors, is the energy separating the delocalised sites from the localised sites in the conduction or valence bands. Monroe [18] first introduced the concept of the transport energy for hopping transport in an exponential DOS. This was later shown to apply to hopping transport in a Gaussian DOS [21].

Charge carriers must be added to organic semiconductors due to the intrinsically low charge carrier densities in these materials. This can occur by injection, photocarrier generation, or doping. The characteristically low mobilities and disordered nature of the materials are issues for charge carrier transport through the material. Organic semiconductors can typically transport one type of charge easier than the other. In the case of conjugated polymers, for example, most of the materials behave as p-type materials and if ambipolar transport is observed, hole mobilities are usually orders of magnitudes larger than electron mobilities. This is attributed to traps in the material that impede the electron transport [22]. Recently, however, time of flight (ToF) measurements on purified regioregular poly(3-hexylthiophene) films have revealed electron and hole mobilities in the same order of magnitude [23].

The process of charge carrier injection into organic semiconductors as well as the physics at the metal-semiconductor interface are still not well understood, and are discussed in the next section.

Chapter 2

Investigating charge transport in organic diodes

2.1 Organic light emitting diodes (OLEDs)

A breakthrough in the field of organic light emitting diodes (OLED) was reported by Tang et al. [24] in 1987, using Alq_3 as the organic semiconducting layer. The energy diagram of an organic light emitting diode (OLED) is shown in figure 2.1 a). The contacts are chosen so that the anode is a high work function metal that will form an ohmic contact with the Highest Occupied Molecular Orbital (HOMO) for efficient hole injection into the semiconductor, and the electrode is a low work function metal that will form an ohmic contact with the Lowest Occupied Molecular Orbital (LUMO) for electron injection. Electroluminescence was observed in the conjugated polymer poly(paraphenylene vinylene) (PPV) in 1989 [25], and the energy levels in the diagram are taken from the PPV OLED. A layer of poly-ethylene dioxythiophene:poly-styrene sulphonic acid (PEDOT:PSS) is used to improve the hole injection conditions [26; 27]. The chemical structure of PPV is shown in figure 2.1 b). Light, with a wavelength corresponding to the HOMO-LUMO gap, is emitted from the diode when the charge carriers recombine within the device.

OLEDs are extremely good candidates for display technologies. OLED displays are potentially cheap, energy efficient, light-weight and thin; only a driving voltage is needed across the panel instead of back lighting. The displays have a large viewing angle and good resolution. OLED displays appeared on the market

2.2 Space charge limited currents (SCLC)

in 1999 when Pioneer introduced a multi-colour small molecule OLED car stereo display. In 2002, Phillips brought out a polymer LED (polyLED) monochrome display for an electric razor (courtesy of Phillips Research: Polymer light emitting diodes). Since then OLED displays have made their way into cell phones, and car components, and larger prototype displays exist. Limiting factors for the performance of OLED and polyLED displays remain the efficiencies of the devices and the stability of the organic materials, however considerable progress has been made on these fronts [28].

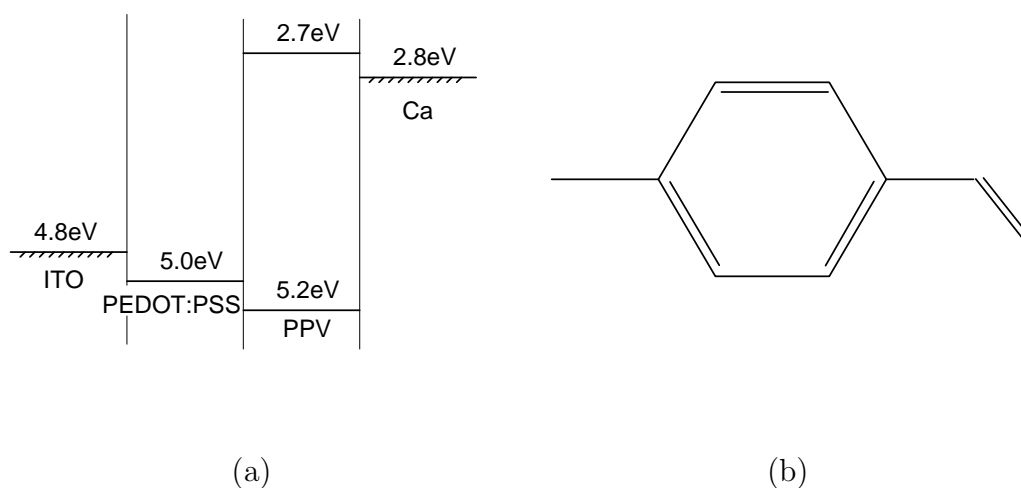


Figure 2.1: a) Energy diagram of an organic light emitting diode. b) Chemical structure of PPV.

2.2 Space charge limited currents (SCLC)

It is possible to investigate the transport properties of one type of charge carrier in a diode structure by choosing metals with appropriate work functions for the contacts. If, for example, two high work function metals are used to form ohmic contacts with the HOMO level of the semiconductor, a “single carrier” device is made in which hole transport in the semiconductor can be investigated.

The charge carrier mobilities in organic semiconductors are typically low. In the case that the injection barriers between the metal and semiconductor are

2.2 Space charge limited currents (SCLC)

small, and charges can be efficiently injected into the device, the device limiting factor is the ability of the material to transport the charge through the bulk. Using the concept of the transport energy introduced in section 1.3, charge transport in such devices can be described using the theory for SCLC [29] in the presence of multiple trapping and release [30].

The Poisson equation describes the relationship between the electric field and the local charge density,

$$\frac{dF}{dx} = \frac{q}{\epsilon_o \epsilon_r} (p_c(x) + p_t(x)), \quad (2.1)$$

where q is the elementary charge, ϵ_o is the permittivity of free space, and ϵ_r is the dielectric constant of the material. The total density of carriers is given by $p(x) = p_c(x) + p_t(x)$, where $p_c(x)$ is the density of carriers in conductive states, and $p_t(x)$ is the density of carriers in trapped states.

The current density is given by

$$j = q\mu(F)F(x)p_c(x), \quad (2.2)$$

where $\mu(F)$ is the field dependent mobility.

When the system is in equilibrium, the density of trapped charge carriers is given by the Gaussian DOS, and the Fermi-Dirac distribution according to

$$p_t(x) = \int_0^\infty \frac{g(E)}{1 + \exp\left[-\frac{E-E_F}{k_B T}\right]} dE, \quad (2.3)$$

where $E = 0$ corresponds to the mobility edge.

Equations (2.1) and (2.2) can be combined to give the current-voltage (IV) relation

$$\frac{dF(x)}{dx} = \frac{j}{\epsilon_o \epsilon_r \mu(F) F(x)} + \frac{q}{\epsilon_o \epsilon_r} p_t(x), \quad (2.4)$$

2.2 Space charge limited currents (SCLC)

To obtain the IV characteristics from (2.4), the differential equation has to be solved numerically according to the boundary equation $F(0) = 0$. The voltage is given by $V = \int_0^L F(x)dx$, where L is the thickness of the semiconducting layer.

2.2.1 Determining charge carrier mobilities from SCLC measurements

It is possible to determine the charge carrier mobility from the SCLC behaviour discussed in the previous section. In the limiting case that the mobility is assumed to be not strongly field dependent, and trapping is ignored so that only the free charge carriers are considered, equation (2.4) is rewritten as [31; 32]

$$j = qp_c\epsilon_o\epsilon_r\mu F(x)\frac{dF(x)}{dx}. \quad (2.5)$$

Integrating equation (2.5) from $x = 0$ to L results in the Mott-Gurney law [29]

$$j = \frac{9}{8}qp_c\mu\epsilon_r\epsilon_o\frac{V^2}{L^3}. \quad (2.6)$$

At lower voltages the IV characteristics follow the Ohmic behaviour given by eq. (2.2). At higher voltages, the SCLC behaviour becomes apparent, and the IV characteristics follow eq. (2.5). The transition is marked by a change in the slope in the graph of the IV characteristics from slope = 1 to slope = 2, and the mobility can be determined at this point from the two expressions.

Much work has been done to expand the SCLC model to include the field dependence of the mobility and trapping effects [32; 33; 34; 35].

2.2.2 The SCLC Model in combination with other effects

In the literature charge transport in organic diodes is often described with the SCLC model in combination with other effects, as the SCLC model alone may not be sufficient to describe charge transport in the device if other processes or phenomena dominate device behaviour. Some of the common variations to the SCLC model found in the literature for organic devices are reviewed.

2.2.2.1 Distribution of traps

Chemical impurities and/or unintentional doping mechanisms along with structural irregularities can lead to traps for charge carriers in organic semiconductors. A Gaussian DOS used to account for the initial disorder inherent to the organic semiconductor superimposed with a second Gaussian DOS to account for the effect of impurities leads to a DOS with a double Gaussian peak [36]:

$$g(E) = \frac{N - N_t}{\sqrt{2\pi}\sigma} \exp\left(-\frac{E^2}{2\sigma^2}\right) + \frac{N_t}{\sqrt{2\pi}\sigma_t} \exp\left(-\frac{(E - E_t)^2}{2\sigma_t^2}\right), \quad (2.7)$$

where N is the total density of states, N_t is the density of trapped states, σ is the width of the distribution, σ_t is the width of the distribution of traps, and E_t is the average trap energy. In addition, $N_t \ll N$ and $\sigma_t \gg \sigma$. The impurities are typically found at deeper energies than the transport sites.

2.2.2.2 Recombination

It is assumed that if the metal contacts are chosen appropriately, there will only be one type of charge carrier in the device. It is possible, however, that at high voltages or temperatures, charge carriers of the opposite type will be injected into the material. This can result in charge carrier recombination in the device, leading to a lower effective current. In the case of PPV, OLEDs can be fabricated with a low work function metal as the cathode to inject electrons into the LUMO level of the polymer, as was discussed in the previous section. However, even in the case of lower work function metals (eg, aluminum [37]) the magnitudes of the electron currents are expected to be very small compared to the hole currents [35]: one of the limiting factors for PPV based OLEDs is the unbalanced hole and electron currents in the device, a fact which led to the introduction of hole blocking layers for more efficient devices [38].

2.2.2.3 Built-in potential

In the metal-insulator-metal picture (MIM) [39], when a semiconductor is brought into contact with a metal, band bending will occur. In the case of an organic

2.3 Example of SCLC currents in polymer diodes

semiconductor, the material is depleted of charges when the device is under equilibrium conditions, and the band bending will result in a tilting of the HOMO-LUMO levels between the metal contacts, as shown in figure 2.2. The result is a built-in potential across the diode [40; 41]. The built-in potential has to be overcome by the applied voltage before the device will operate.

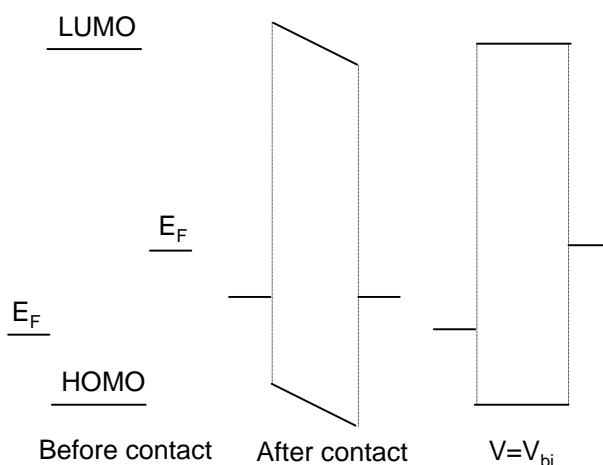


Figure 2.2: Left: energy levels of the metal contacts and the semiconductor before contact. Middle: energy diagram of a diode in equilibrium with band tilting effects. Right: energy diagram of a diode when a voltage equal to the built-in field is applied across the device.

2.3 Example of SCLC currents in polymer diodes

The current density-voltage JV characteristics for poly[2-methoxy,5 ethyl(2'hexyloxy) paraphenylenevinylene] (MEH-PPV) diodes [42] were investigated according to the SCLC model. The structure of the diode is the same as shown in figure 2.1. The anode is a sputtered layer of indium tin oxide (ITO), with a layer of PEDOT:PSS spun over top. The cathodes were varied between samples: Cu, Au, Al.

Figure 2.3 a) shows the experimental current-voltage (JV) characteristics for the diodes. The devices are assumed to be hole only devices. Holes are injected from the ITO:PEDOT anode and are extracted from the device at the cathode. It

2.3 Example of SCLC currents in polymer diodes

is unclear why the shape of the IV curves is dependent on the metal used for the cathode when the device behaviour is analysed solely based on the SCLC model, as the cathode should have little effect on the behaviour of the hole only device. In an attempt to explain this, the experimental data from the MEH-PPV diodes

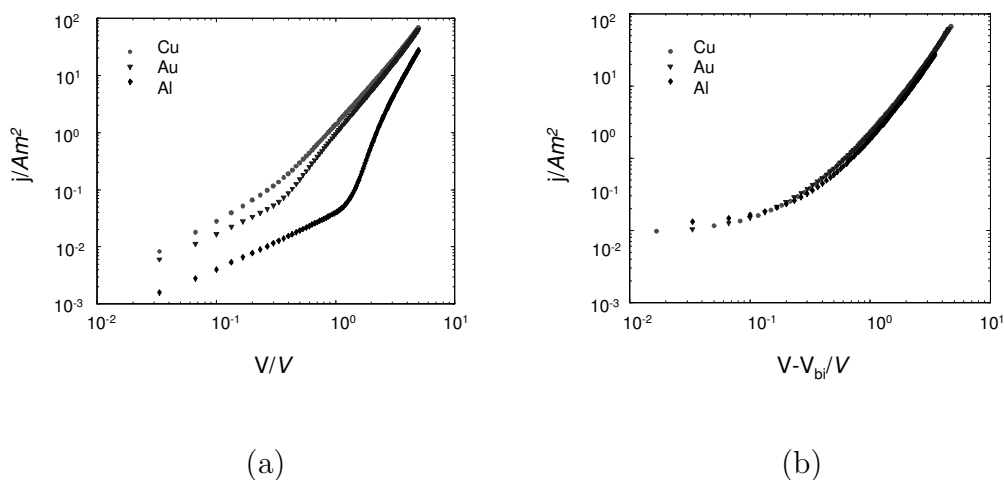


Figure 2.3: a) JV characteristics for MEH-PPV diodes with Au, Cu, and Al electrodes [42]. b) JV characteristics for MEH-PPV diodes with Au, Cu and Al electrodes once the built-in field has been considered [42].

was then investigated with the SCLC model in combination with the effects of: a distribution of deep traps, recombination effects due to electron injection, and the built-in field across the diode. It was found that the IV characteristics of the diodes could best be explained by a simple SCLC model with a field dependent mobility and a built-in field [42]. Figure 2.3 b) shows the IV characteristics once the built-in field has been accounted for. The apparent cathode dependence of the IV characteristics is no longer present.

Until now it was assumed that the injecting contact forms an ohmic contact with the semiconductor. In the next section, charge carrier injection models commonly found in the literature are reviewed.

Chapter 3

Charge carrier injection in organic semiconducting devices

The injection from metal into semiconductor is still poorly understood, and a deeper knowledge of the dynamics at the metal-semiconductor interface is one of the keys to improving device performance. As organic semiconductors intrinsically have no free charge carriers, charge carrier injection is one of the major steps in charge transport through an organic device. Inefficient injection or extraction of charge will hamper the device performance. In this section the metal-semiconductor interface is discussed, including the injection barrier and dynamics between the metal and semiconductor. Then some injection models are reviewed, as well as experimental work relating to isolating and investigating the charge carrier injection processes in organic semiconducting devices.

3.1 Injection barrier heights

As a general rule, the currents in organic devices with injection barriers greater than 0.25 - 0.3eV [1] (this value is considered at zero field, without the effects of electric field induced barrier lowering) are found to be “injection limited”, ie the injection process is the current limiting factor in the device, as opposed to “bulk limited” devices in which factors in the semiconducting bulk limit current and dominate device characteristics. This means that the only deciding factor between injection limited and bulk limited transport is the height of the injection barrier [20].

Injection barriers can be difficult to estimate based on the work function of the metal and the energy levels of the semiconductor alone. Actual injection barrier heights can vary quite strongly from the expected values. In the literature, the deviation between experimentally determined and expected values for the injection barrier height are attributed to chemical reactions between the metal and semiconductor leading to interface dipoles [43; 44], band bending [45; 46] or Fermi level pinning [47].

3.2 Injection models

Until the mid 90's injection models from inorganic semiconductor physics, such as Richardson-Schottky (RS) thermionic emission [48; 49] and Fowler-Nordheim (FN) field emission [50], were often employed to describe the injection process into organic devices. The probability of a charge carrier quantum mechanically tunnelling through a triangular barrier into a delocalised continuum of energy states can be calculated from the WKB (Wigner, Kramers, Brillouin) approximation. The FN model describes tunnelling currents at high electric fields or high injection barrier heights as a function of the electric field across the device and the tunnelling probability. At high temperatures or low injection barrier heights, RS thermionic emission predicts the injection of a charge carrier from a metal contact into a semiconductor if the thermal energy of the carrier is greater than the Schottky barrier height. Hybrid models such as thermally assisted field emission or field assisted thermionic emission also exist to describe the transition region between field emission and thermionic emission.

When applied to organic semiconductors the FN model was successful to some extent in describing the shape of IV curves of some organic diodes [51; 52]. The predicted injection currents were found to differ from the experimental values by several orders of magnitude [53], however, without any physical explanation. The basis of tunnelling into band structures within the semiconductor is also not consistent with the knowledge of the amorphous nature of these materials.

In 1965 Simmons [54] demonstrated that the Richardson-Schottky equation is not sufficient for describing thermionic emission currents into low mobility materials. The equation was rederived with consideration of the short electronic

mean free path, and the results yielded a mobility and electric field dependent thermionic emission injection current. In 1966 Emtage et al. [55] expanded on these results to include bulk effects. Their findings are illustrated by injection currents in organic devices experimentally found to be many orders of magnitude lower than those predicted by the RS model, deviations from the expected temperature dependence [56], and mobility dependent injection currents observed in organic devices [57].

In the mid 90's, new injection models began to emerge that took the disordered energetic structure of organic semiconductors into account. The list is long, but here some of the more common models found in the literature are presented. In 1995, Abkowitz et al. [58] proposed an injection model in which charge carriers undergo a thermally assisted tunnelling from the Fermi level of the metal contact to localised sites within the organic semiconductor. The results from the model were found to successfully describe the temperature and injecting contact dependent current-voltage characteristics in a polytetraphenylbenzidine polymer.

In 1997, Conwell et al. [59] proposed an injection model for charge carrier tunnelling into polaron levels. The position of the polaron levels are not given by the HOMO and LUMO levels but depend on the conjugation length of the polymer, which varies between polymer chains.

In 1998 Arkhipov et al. [60] proposed an analytical model for injection into a Gaussian DOS. The model is broken into two electric field and temperature dependent steps: charge carriers make an initial hop from the Fermi level of the metal contact into the tail states of the distribution followed by an diffusive Onsager-like process. In 1999 a detailed three-part study investigating charge carrier injection into disordered materials was performed based on this model. A Monte Carlo simulation was carried out by Wolf et al. [61]. Charge carrier injection from a metal into a disordered system described with a Gaussian DOS via hopping was simulated, where the significant simulation parameters were the width of the Gaussian DOS and the injection barrier height. The results of the simulation were compared to the analytical model from Arkhipov et al. [62], and to experimental data from measurements on vacuum deposited 8-hydroxyquinoline aluminum (Alq_3) diodes [63].

3.3 Experimental studies of charge carrier injection into organic semiconductors

In 1999, Scott and Malliaras [64] used an alternative approach to rederive the results for the diffusion limited thermionic emission model from Simmons and Emtage et al. for organic semiconductors.

Here some of the progresses made towards understanding charge carrier injection into organic devices have been highlighted. Based on electrical measurements alone it can be challenging to distinguish between the results predicted by individual injection models. Only more experimental work in this area can shed more light on this topic. It is accepted, however, that a successful injection model must be able to describe the temperature, electric field, mobility, and charge density dependence observed in injection currents, as well as interface effects such as the image potential and trapping [65].

3.3 Experimental studies of charge carrier injection into organic semiconductors

Experimental studies that isolate the injection processes in organic semiconducting devices and/or deliver information about the metal-semiconductor interface are extremely helpful in furthering the understanding of injection into organic semiconductors. Unfortunately the number of these studies is low, as it can be difficult to separate the injection characteristics from the bulk effects; indeed they are to a good degree co-dependent.

3.3.1 Investigations of the injection efficiency of a contact

Abkowitz et al. [66; 67] showed that it is possible to determine the injection efficiency of a contact by comparing small signal time of flight (TOF) measurements with the space charge limited current (SCLC) behaviour of a trap free organic semiconductor in the diode structure. The premise is that the condition required to observe TOF transients in a device is the same condition that leads to the onset of trap free SCLC behaviour. The injection efficiency, $\eta_{injection}$, can then be determined by $\eta_{injection} = J_{TOF}/J_{TF SCLC}$ [68], where J_{TOF} is the signal from the TOF measurement and J_{SCLC} is the signal from the IV measurements made on the same device and taken at the same voltage.

3.3 Experimental studies of charge carrier injection into organic semiconductors

Using this technique in a later study [68] it was demonstrated that injecting contacts can evolve over time from emission limited to ohmic in polymer devices with Au contacts, a phenomenon that could not be attributed to diffusion of metal atoms into the semiconducting layer, but rather, was imputed to both short term (hours) and long term (months) reconfiguration of the polymer at the interface with the contact.

3.3.2 Investigations of charge carrier injection via contact effects in organic field effect transistors

The contact effects in organic field effect transistors (OFETs) have also been used to investigate charge injection into organic semiconductors. It has been shown that the contact resistances in OFETs are temperature and field activated [69; 70; 71], like the field effect mobility, and in fact that the contact resistance varies inversely with the mobility with comparable activation energies [69; 71]. The injection characteristics from the source contact into the channel is the commonality. An injection current described by diffusion limited thermionic emission (DLTE) is suggested by these findings. According to the DLTE model [54; 55; 64], the injection current is given by

$$j_{inj} = 4q\psi^2 N \mu F \exp\left(-\frac{\phi_B - \Delta\phi}{k_B T}\right), \quad (3.1)$$

where ψ is a slowly varying function of the electric field, N is the density of states, F is the electric field, ϕ_B is the height of the injection barrier from metal into semiconductor, and $\Delta\phi$ is the term due to Schottky barrier lowering.

Microscopic studies [65; 69] on OFETs by means of non-contact scanning probe potentiometry, however, revealed some discrepancies between the DLTE model and the experimental results when the theory was strictly applied. It was found that the effective injection barrier height predicted by the model was too large to explain the experimental data. This indicates that either other injection mechanisms are at hand, such as tunnelling, or that the disorder in the system must be considered here, as a disorder term results in a reduced effective barrier height given by $\phi_b - \Delta\phi - \sigma^2/kT$ [60; 69; 72].

3.3 Experimental studies of charge carrier injection into organic semiconductors

In the next section, it is shown that the current-voltage characteristics of a contact limited fullerene OFET can be well described using the DLTE model when the disorder of the system is accounted for.

3.3.3 Bilayers for efficient charge injection

The efficient injection of electrons into organic semiconductors remains an issue, as in order to inject electrons into the LUMO level of an organic semiconductor lower work function metals (Ca, Mg, Al) must be used as contacts. These metals are instable, however, and oxidise quickly and react with the organic layer [73], which can lead to unexpectedly high injection barrier heights for charge carrier injection. It was found that using a bilayer of LiF or MgO between the organic material and metal contact could improve the electron injection efficiency considerably in some devices [74]. Similar improved device behaviour due to bilayer effects have been observed for electrodes deposited in the presence of some oxygen, resulting in a thin insulating layer between the contact and semiconductor, which may serve to prevent a direct reaction between the cathode and the organic semiconductor [75; 76].

An enhancement in device performance was also observed for bilayers between the anode and semiconducting layer resulting in improved hole injection [77].

Chapter 4

Charge transport in organic field effect transistors (OFETs)

4.1 Background

The transistor is one of the most important building blocks in the modern-day world. The advantages of organic semiconductors have already been mentioned, however in the field of transistor technology, the potential to produce smaller, cheaper, faster electronics that can be processed at low temperatures and on flexible substrates is especially significant.

The transistor was invented in 1947 by Shockley, Brattain and Bardeen. It can operate as a switch or an amplifier, and is a major component in all digital electronics. The first silicon field effect transistor [78] appeared in 1960. The field effect was being investigated in organic semiconductors just a decade later, in 1970 [79; 80]. The first actual OFET device was reported in 1987 [81], and since then, there has been a lot of progress made towards the technological development of the organic based devices as well as the understanding of the physics behind them. OFETs are candidates for, among other things, complementary circuits [82], ring oscillators [83], low-end display driving circuits [84; 85], chemical sensors [86], and integrated circuits [87; 88]. The first light emitting OFETs have recently been reported [89]. Many good reviews have been written about the state of the art of OFET technology [90; 91] and single crystal OFETs [92].

Generally, the charge carrier mobilities in organic semiconducting films are lower than those in inorganic semiconductors. Single crystal OFETs, however,

are quicker, smaller and offer higher mobilities than thin film OFETs. Mobilities in rubrene single crystal transistors have been reported to be as high as $15.4 \text{ cm}^2/\text{Vs}$ [93]. These are higher than the mobilities found in amorphous silicon thin film transistors.

In addition to the technological side, OFETs offer a good method to investigate the charge transport properties of organic semiconductors by means of direct investigation of the electric field and temperature dependence of the mobility. This point has been called into question by some researchers [92; 94] regarding the thin film OFETs. Impurities in the chemical structure or defects in the semiconducting film [95], contact effects, and general artifacts from processing can seriously effect the output characteristics of these devices. Mobility measurements via single crystal OFETs are thought to give more accurate information on charge carrier mobilities and transport characteristics. However, the point should be made that sometimes the general transport conditions in the film *are* the focus of interest. Changes in the charge carrier field effect mobility can indicate changes in the quality of the film. This is a potential method to screen processing conditions of films, such as the solvent used, the concentration of the solution, parameters for tempering, etc. Mobility measurements can be made on blends of semiconducting materials in the OFET structure, and the mobilities of both charge carrier types can be determined from the same device. Changes in the morphology of multi-component organic layers, for example in the films used for bulk-heterojunction polymer-fullerene solar cells, can be easily detected with field effect measurements. In many cases, improving the morphology of solution processed organic semiconducting films remains one of the obstacles for improving device performance.

4.2 FET structures

An FET is a three (or more) terminal device. A voltage applied to the gate electrode is used to form a conductive channel in a semiconductor. The channel is contacted by the source and the drain contacts. There are several variations of the FET structure, including the metal-oxide/insulator-semiconductor FET (MOSFET or MISFET), the metal-semiconductor FET (MESFET), the junction

FET (JFET), and the thin film transistor (TFT). The description of the current-voltage characteristics vary depending on the structure of the device [5].

4.2.1 Metal-Oxide-Semiconductor FETs (MOSFETs)

It is worth spending a bit of time reviewing the basic principals behind the MOSFET before discussing the OFET. The TFT structure used for OFETs is a simplification of the MOSFET structure, although the description of the charge transport in the OFET is arguably more complex. The most commonly used transistors today are MOSFETS. The source and drain contacts are n-type (p-type) and are patterned onto a p-type (n-type) substrate. The gate electrode is isolated from the rest of the device by a metal oxide insulating layer. The device behaves essentially as a parallel plate capacitor, where the gate and semiconductor are the plates. Figure 4.1 shows the structure of a MOSFET.

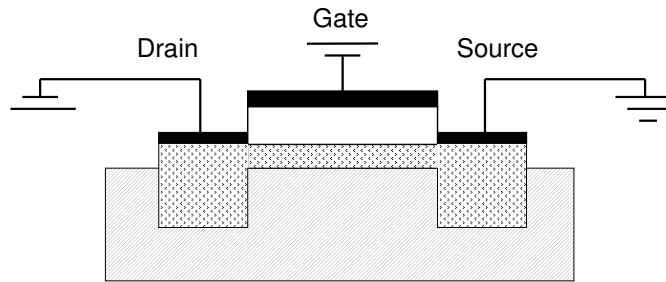


Figure 4.1: Structure of a MOSFET: the gate electrode is separated from the source and drain by an insulating layer (white layer). The source and drain are n-type (p-type) patterned on a p-type (n-type) substrate, and are contacted with ohmic contacts resulting in a three terminal device.

The gate, gate insulator, and semiconductor in a MOSFET behave like a MOS diode. Applying a voltage will cause charge carriers to accumulate below the gate

oxide. The density of charge carriers depends on the sign and magnitude of the voltage. The energy diagram of an ideal p-type MOS diode in the accumulation ($V < 0$), depletion ($V > 0$), and inversion ($V \gg 0$) modes is shown in figure 4.2. Applying a negative gate voltage (V_{gs}) results in the accumulation of holes at the semiconductor-insulator interface and the device is in accumulation mode, fig. 4.2 a). The current in a MOSFET, however, is made up of minority charge

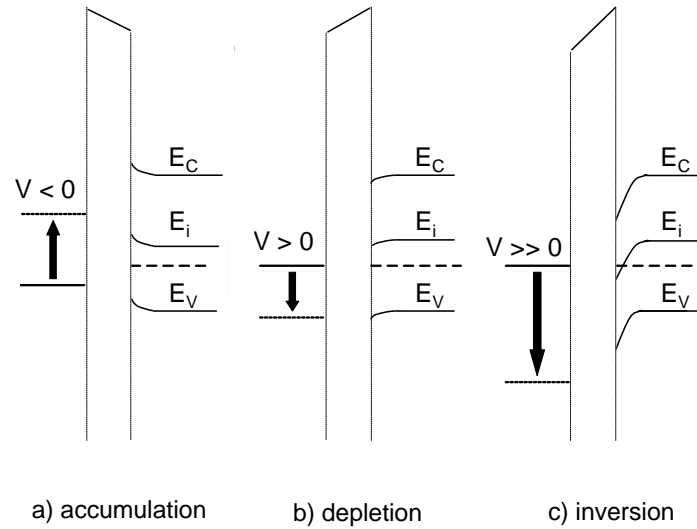


Figure 4.2: Energy diagram of a MOS diode in a) accumulation b) depletion and c) inversion modes when a voltage, V , is applied. E_C is the conduction band, E_V the valence band, and E_i the intrinsic Fermi level. The dashed line represents the Fermi level.

carriers. When a small positive gate voltage (V_{gs}) is applied to a p-type (substrate) MOSFET, some electrons are attracted to the semiconductor-insulator interface and the holes are repelled. The device is in depletion mode, fig. 4.2 b), as the majority charges are depleted in the semiconductor-insulator region. The low voltage only results in a low density of electrons at the interface and no conductive channel is formed between the source and drain contacts. The device is off. Applying a higher positive V_{gs} will induce a transition in the device from the depletion mode into the inversion mode as shown in fig. 4.2 c), turning the

device on. In the inversion mode, the intrinsic Fermi level will cross the Fermi level. The electron density is then higher than the hole density and a conductive n-type channel forms. The gate voltage at which the transition between depletion and inversion modes occurs is called the threshold voltage.

The gate voltage controls the charge density in the channel. For a current to flow in the device, however, a drain-source (V_{ds}) voltage must be applied. Applying a positive voltage to the drain will result in a channel current (I_{ds}), as well as a decrease in the charge density in the region around the drain contact.

The current-voltage characteristics of the MOSFET are calculated according to the gradual channel, or Shockley approximation, for a field independent mobility. The Shockley approximation is based on the assumption that the variation in the electric field due to V_{ds} is much smaller than the variation in the field due to V_{gs} . This assumption is justified as the thickness of the gate insulator is in the order of nanometers while the channel length is in the order of micrometers [5].

For lower V_{ds} , the I_{ds} follows an ohmic behaviour which can be described by

$$I_{ds} = \frac{W}{L} \mu_{FE} C_i (V_{gs} - V_t) V_{ds}, \quad (4.1)$$

where W is the width of the channel, L is the length of the channel, μ_{FE} is the field effect mobility, C_i is the capacitance of the insulating layer, and V_t is the threshold voltage.

Eventually, at higher V_{ds} , the charge density becomes very low in the region around the drain contact. Increasing the gate voltage still results in higher currents, as the gate voltage controls the density in the conductive channel, but the current is no longer dependent on V_{ds} and saturates. This V_{ds} is known as the pinch-off voltage. The saturation current can be described by

$$I_{ds} = \frac{W}{2L} \mu_{FE} C_i (V_{gs} - V_t)^2. \quad (4.2)$$

An example of FET output is shown in figure 4.3 [5].

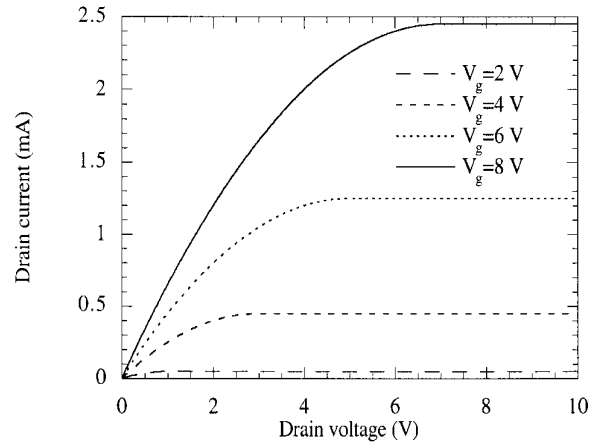


Figure 4.3: The output characteristics of a MOSFET [5].

4.3 OFETs

4.3.1 Structure and current-voltage characteristics of OFETs

OFETs make use of the TFT structure which is suitable for low conductivity materials. Two variations of this structure are shown in figure 4.4. Often highly doped silicon substrates are used as the gate electrode and SiO_2 is used as the gate insulator. The source and drain contacts are metals and are deposited either directly onto the gate insulator for the bottom contact structure, fig. 4.4 a), or as a final step, onto the semiconductor for the top contact structure, fig. 4.4 b). Like the MOSFET, the OFET is a two dimensional device, ie the thickness of the semiconducting layer does not influence the output of the device.

The bottom contact OFET structure is more practical from the point of view of device processing than the top contact OFET structure, as the contacts can be deposited or patterned directly onto the substrate, and the semiconducting layer is applied as the final step. The risk of damaging the sensitive material during contact deposition is reduced. It was found, however, that this geometry results in higher electrical losses at the contacts than the top contact OFET configuration [96; 97]. This has been attributed to the decreased effective injection/extraction contact area in the bottom contact structure due to the minimised source/drain and gate electrode overlap [97].

In contrast to the MOSFET, the OFET operates in accumulation mode and the current is made up of majority charge carriers. For a p-type OFET, applying $V_{gs} < 0$ will cause an accumulation of holes near the semiconductor-insulator interface (fig. 4.2 a). Applying $V_{ds} < 0$ will cause a current to flow across the channel. The device is then in principal turned on for any $V_{gs} < 0$, but the actual on/off behaviour is controlled by the low conductivity of the materials, ie no current is observed at lower V_{gs} . This means that the concept of the threshold voltage does not strictly apply to OFETs [98]. In contrast, some organic semiconductors have been observed to always exhibit on behaviour, even when no gate voltage is applied, something that is attributed to doping effects in the organic semiconducting layer [99; 100].

Figure 4.5 shows the FET characteristics of a fullerene OFET.

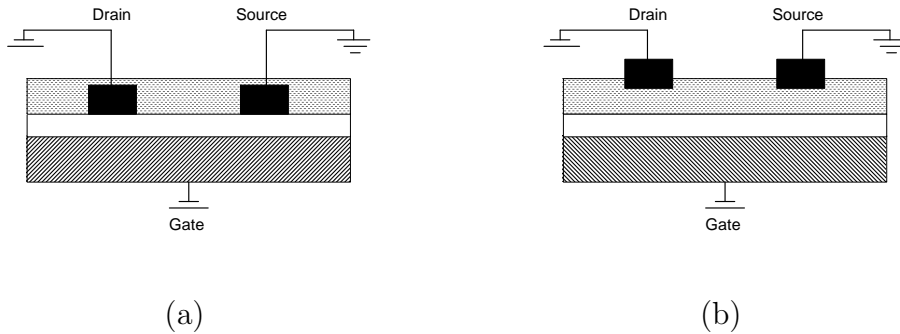


Figure 4.4: a) Bottom contact OFET structure: the source and drain contact are deposited onto the gate oxide and the semiconductor is applied as the final step. b) Top contact OFET structure: the source and drain contacts are deposited onto the semiconducting layer

4.3.2 The field effect mobility

The field effect mobility can be determined from the ohmic region of the IV characteristics of an OFET according to equation (4.1) [101]

$$\frac{\partial I_{ds}}{\partial V_{gs}} = \mu_{FE} W C_i V_{ds} / L. \quad (4.3)$$

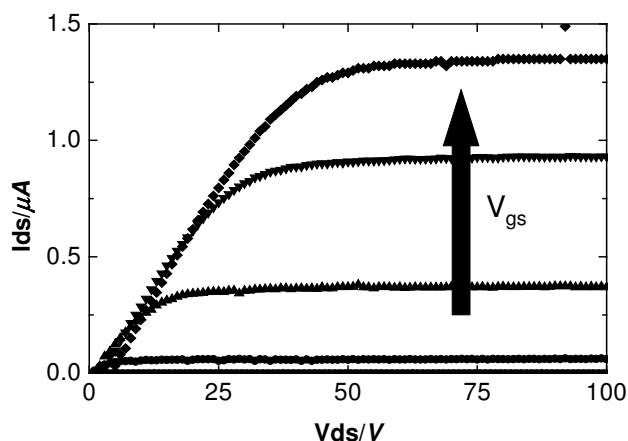


Figure 4.5: The source-drain current voltage characteristics of a fullerene OFET for various gate voltages.

According to equation (4.2), it is also possible to determine the mobility from the saturation region of the IV characteristics. It should be noted again though that equations (4.1) and (4.2) are derived assuming a field independent mobility. As charge carrier mobilities in organic semiconductors are known to be field dependent, the assumption of constant mobility may be well approximated for the lower voltages in the linear regime of the IV characteristics, but will not hold for the higher fields in the saturation regime [5].

Mobility measurements determined via field effect measurements are found to be comparable to those determined from TOF measurements, but orders of magnitude larger than those determined by SCLC measurements. This is due to the strong field and temperature dependence of the charge carrier mobilities in organic semiconductors. SCLC measurements are performed at lower fields and charge carrier densities [102].

4.3.3 The Meyer-Neldel rule in OFETs

The conductivity in organic semiconductors demonstrates an Arrhenius-like behaviour. This behaviour is also seen in the charge carrier mobilities:

$$\mu = \mu_o \exp\left(\frac{-E_a}{k_B T}\right), \quad (4.4)$$

where E_a is the activation energy, k_B is Boltzmann's constant, and T is the sample temperature. It has been found for many materials that μ_o is not a constant, but depends exponentially on the activation energy [103], a behaviour known as the Meyer-Neldel (MN) rule

$$\mu_o = \mu_{oo} \exp\left(\frac{E_a}{k_B T_o}\right), \quad (4.5)$$

where μ_{oo} and T_o are material constants.

The physical origin of the MN rule remains unclear. Some models predict MN behaviour due to an exponential distribution of defect states within the material [104; 105], where T_o represents the width of the distribution of traps. Jackson [106] demonstrated that the MN rule should be observed whenever charge transport is dominated by multiple trapping and release processes. Generally, the phenomenon is attributed to disorder within the material.

The general expression for the mobility according to the MN rule is then given by:

$$\mu_{FE} = \mu_{oo} \exp\left(-E_a \left[\frac{1}{k_B T} - \frac{1}{k_B T_o}\right]\right). \quad (4.6)$$

This behaviour has been observed in many organic semiconductors. The MN rule was observed for the conductivity in fullerenes by several groups, and a strong correlation between the constant prefactor μ_{oo} and T_o was found to exist [107; 108]. A study in 2000 demonstrated that the MN rule could be observed in the field effect mobility of a variety of different organic semiconductors, and the MN activation energies between the materials were found to be surprisingly similar [109].

4.4 Modelling charge transport in OFETs

A model was proposed by Vissenberg and Matters [110] which describes the field effect mobility in amorphous organic semiconductors. The model is based on variable range hopping in an exponential DOS:

$$g(E) = \frac{N}{k_B T_{DOS}} \exp\left(-\frac{E}{k_B T_{DOS}}\right), \quad (4.7)$$

where T_{DOS} is the width of the distribution. Although transport in organic semiconductors is typically described by hopping transport within a Gaussian DOS, the Gaussian DOS prevents closed analytical solutions [15]. It was demonstrated that over the energy regime in which OFETs operate, the Gaussian DOS with a width of σ can be approximated well by an exponential DOS with an appropriate value of T_{DOS} [102].

Using percolation theory, an analytical expression for the temperature and field dependent conductivity was found [110]

$$\sigma(\delta, T) = \sigma_o \left(\frac{\pi N \delta (T_{DOS}/T)^3}{(2\alpha)^3 B_c \Gamma(1 - T/T_{DOS}) \Gamma(1 + T/T_{DOS})} \right)^{T_o/T}, \quad (4.8)$$

where σ is the conductivity, δ is the carrier occupation, σ_o is a prefactor for the conductivity, α^{-1} which is a factor representing the overlap between sites, Γ is the gamma function, and B_c is the critical number for the percolation onset, which is taken as 2.8 for 3d amorphous media [110; 111].

Based on these results, the IV characteristics and field effect mobility of amorphous organic semiconductors could be described by integrating equation (4.8) over the channel length.

The I_{ds} versus V_{gs} characteristics are given by [99; 110]

$$I_{ds} = \frac{W V_{ds} \epsilon_o \epsilon_r \sigma_o}{L q} \left(\frac{T}{2T_{DOS} - T} \right) \sqrt{\frac{2k_B T_{DOS}}{\epsilon_o \epsilon_r}} \times \left(\frac{(T_{DOS}/T)^4 \sin(\pi T/T_{DOS})}{(2\alpha)^3 B_c} \right)^{\frac{T_{DOS}}{T}} \left(\sqrt{\frac{\epsilon_o \epsilon_r}{2k_B T_{DOS}}} \left[\frac{C_i(V_{gs})}{\epsilon_o \epsilon_r} \right] \right)^{\frac{2T_{DOS}}{T} - 1}. \quad (4.9)$$

The constants are: ϵ_o is the permittivity of free space, ϵ_r is the permittivity of the semiconductor, and q is the elementary charge.

The field effect mobility is given by equations (4.1) and (4.9) [110]

$$\mu_{FE} = \frac{\sigma_o}{q} \left(\frac{\pi(T_{DOS}/T)^3}{(2\alpha)^3 B_c \Gamma(1 - T/T_{DOS}) \Gamma(1 + T/T_{DOS})} \right)^{\frac{T_{DOS}}{T}} \times \left(\frac{C_i(V_{gs})^2}{2\epsilon_o\epsilon_r k_B T_{DOS}} \right)^{\frac{T_{DOS}}{T} - 1}. \quad (4.10)$$

The parameters σ_o and T_{DOS} have been found to have little effect on the mobility, as these parameters are sometimes very comparable between lower and higher mobility materials. Rather, the overlap parameter α appears to be the deciding factor, as this describes the tunnelling between sites [110].

It can be seen from equations (4.8) and (4.10) that the conductivity and mobility are predicted to follow an Arrhenius type behaviour, consistent with the observed behaviour for organic semiconductors.

The model was shown to describe the field effect behaviour in polymer (PPV and poly(3-hexylthiophene) (P3HT)) and small molecule (pentacene) OFETs [99; 110] well. Later in this chapter, the model is applied to the temperature dependent IV characteristics from a fullerene OFET. First, however, the effects of the contact resistance on the OFET performance is discussed.

4.5 Contact effects in OFETs

OFETs operate with charge carrier densities typically in the order of 10^{20} - 10^{22} /cm³, relatively high compared to those in organic diodes or solar cells. In materials with such low intrinsic charge carrier densities, the injection conditions as well as the dynamics at the interface between the metal and semiconductor can be deciding for device performance as the charges must be injected into the material.

The total device resistance (R_{tot}) is a sum of the resistances between the source and drain contacts and the semiconductor (R_{con}) and the resistance of the semiconducting film across the channel (R_{ch}), and is given by

$$R_{tot} = R_{ch} + R_{con}. \quad (4.11)$$

In the case that the OFET is contact limited ($R_{con} > R_{ch}$), the contact resistance has an impact on the device output. The effects of contact resistances on the performance of silicon thin film transistors (TFTs) is well known [112]. Recently, there has been a lot of focus on the influence of contact resistances on the performance of OFETs. Contact resistances in OFETs at room temperature are often found to be in the $k\Omega$ to the $M\Omega$ range [69; 70; 71; 97], and can affect determined mobility values by up to several magnitudes [71; 113], and as previously mentioned, can be influenced by the geometry of the device [96; 97].

The contact resistance manifests itself as a voltage drop in the drain and source contact regions. This results in an effective voltage drop across the channel, resulting in a lower current. There are several methods that can be employed to determine the magnitude of contact resistances in a device. Some groups have performed studies where the voltage drop across the channel is directly measured by means of conducting probe potentiometry [114], non-contact scanning probe potentiometry [65; 69; 115; 116], or by the four probe method [70; 117].

Another direct method to determine the contact resistance is to vary the channel length between samples. R_{tot} can be determined from the linear region of the I_{ds} versus V_{ds} characteristics for a constant V_{gs} . The total device resistance will increase with increasing channel length, but the contact resistance remains constant between the samples. Plotting the channel length versus device resistance will yield the channel resistance per unit length as the slope, and the contact resistance as the ordinate [70; 71; 113].

With consideration of the contact resistance, equation (4.3) becomes [71]

$$\frac{\partial[(\partial R_{tot}/\partial L)^{-1}]}{\partial V_{gs}} = \mu_{FE}WC_i. \quad (4.12)$$

Contact resistances have been observed to be nonlinear. It was already mentioned in section 3.3 that the contact resistances in OFETs are electric field and temperature activated [69; 70; 71], and that studies of the contact resistances have been used to investigate injection processes in these devices [65; 69; 71].

4.6 Modelling charge transport in fullerene OFETs

The contact resistances have been observed to vary with the electric field and charge carrier mobility, in accordance with injection processes described by DLTE introduced in section 3.3.2. The DLTE model has been found to successfully describe injection into organic semiconductors in many studies [57; 71]. The behaviour of the contact resistance is then given by

$$R_{con} \propto \frac{1}{\mu_{FE}F} \exp\left(\frac{\phi_B - \Delta\phi}{k_B T}\right). \quad (4.13)$$

In the case of the microscopic measurements on contact limited OFETs [65; 69], the effective barrier height predicted by the model is found to be too large to explain the experimental results. It is shown in the next section that accounting for the disorder in the semiconductor results in a good agreement between the predicted injection currents from the DLTE model and experimental data from a contact limited fullerene OFET.

The following form was assumed for the contact resistance according to (4.5), (3.1), and (4.13):

$$R_{con} = \frac{R_{oo}}{F} \exp\left(E_a \left[\frac{1}{k_B T} - \frac{1}{k_B T_o}\right]\right) \exp\left(\frac{(\phi_B - \Delta\phi)}{k_B T}\right), \quad (4.14)$$

where R_{oo} is a constant.

4.6 Modelling charge transport in fullerene OFETs

There has been much more work done on p-type than n-type OFETs. This has partially to do with the sensitivity of n-type materials to oxygen and the lack of suitable n-type materials [118], as well as the instability with respect to oxygen and to organic materials of the low work function metals needed to efficiently inject electrons.

The buckminster fullerene was discovered by accident in 1985 [119], and Curl, Kroto and Smalley were awarded the Nobel Prize in chemistry in 1996 for the significant find. The molecule is made up of 60 carbon atoms (C_{60}) and is spherical in shape. The structure, which is stable in air but chemically active was found

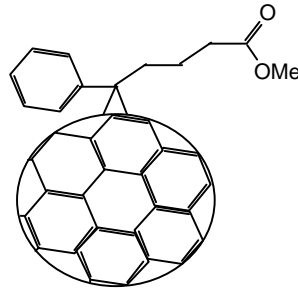


Figure 4.6: Chemical structure of PCBM.

to demonstrate a number of interesting characteristics (for a good overview, see [120]), among them, conductivity. Since the discovery of C_{60} , many variations of fullerenes have been investigated.

The chemical structure of methanofullerene [6,6]-phenyl C_{61} -butyric acid methyl ester (PCBM) is shown in figure 4.6. PCBM is a soluble fullerene derivative. PCBM is an interesting organic semiconductor to investigate for several reasons. It is relatively stable, demonstrates relatively high electron mobilities, and is easily processed due to its solubility. The synthesis of PCBM is described in more detail elsewhere [121].

In this section the field effect characteristics of PCBM OFETs are investigated. First, the electron mobilities at room temperature are discussed. For devices not limited by contact effects mobilities are found to be in the order of $10^{-2} \text{cm}^2/\text{Vs}$. Then, the temperature dependent field effect characteristics for a contact limited PCBM OFET are investigated. The contact resistance is shown to shed some light on the injection mechanisms in these devices. Once contact resistances have been considered, the IV characteristics and electron mobilities of PCBM OFETs can be very well described according to the model for OFET output introduced in section 4.4.

4.6.1 Experimental

The field effect transistors were prepared using highly doped p-Si wafers as the gate electrode. A layer of thermally grown SiO₂ served as the gate insulator. The thickness of the SiO₂ layer was in the order of 100nm. Processing was done under a defined nitrogen atmosphere. All solutions were prepared with chloroform and applied to the wafer via spin coating. Measurements were performed under vacuum and in the dark. Both the top and bottom contact structure OFETs were investigated. A shadow mask was used to form the source and drain contacts, and the contacts were deposited in a deposition chamber at a rate of 0.01 to 0.1 nm/s. The metals used for the source and drain contacts are specified in the text.

Two batches of PCBM were used in these investigations. One batch came from a partner laboratory (the group of J. C. Hummelen at the University of Groningen) and the other was commercially purchased from Nano-C.

4.6.2 Room temperature field effect mobilities

The electron mobilities in PCBM were determined at room temperature. The top contact OFET structure was used to minimize the contact effects for more accurate mobility measurements. The PCBM investigated in this section was donated from the partner laboratory.

Figure 4.7 shows the I_{ds} versus V_{gs} characteristics for a top contact PCBM OFET with Mg contacts, where $L = 85 \mu\text{m}$, $W = 2\text{mm}$, and $V_{ds} = 2\text{V}$. From the slope, the electron mobility was found to be $2.2 \times 10^{-2} \text{cm}^2/\text{Vs}$ using equation (4.3) at a gate voltage of 10V. This value is slightly higher than the typical value of $10^{-3} \text{cm}^2/\text{Vs}$ found for OFET measurements on PCBM in the literature [122; 123], except at higher gate voltages, at which injection conditions are modified resulting in higher mobility estimations [124].

The injection conditions between Mg and PCBM may be expected to deliver optimal results, as the LUMO of PCBM lies around 3.7 eV [125] and the work function of Mg is given to be 3.9 eV in the literature. However, in addition to this, a study done by Chikamatsu et al. [126] on top contact C₆₀ OFETs using secondary-ion mass spectroscopy demonstrated that Mg will dope the C₆₀ layer.

4.6 Modelling charge transport in fullerene OFETs

It was found that the Mg atoms diffused into the semiconducting layer, behaving as electron donors and resulting in higher experimentally determined mobilities.

It is also possible, as mentioned in section 3.3.3, that Mg contacts formed in the presence of oxygen may actually lead to a MgO bilayer between the contact and semiconductor that improves the injection of electrons into the device [75; 76].

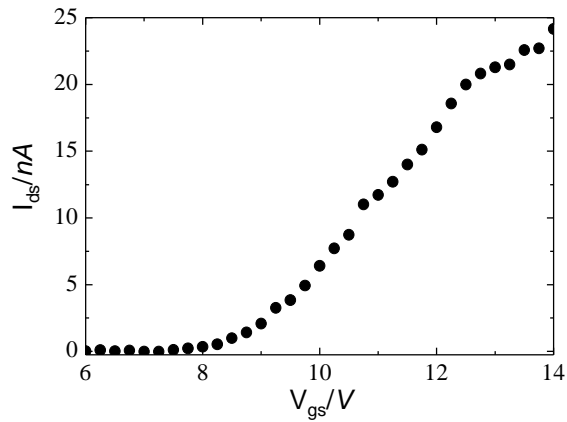


Figure 4.7: I_{ds} versus V_{gs} characteristics for electron transport in a top contact PCBM (partner laboratory) OFET with Mg source-drain contacts. $L = 85 \mu\text{m}$, $W = 2\text{mm}$, and $V_{ds} = 2V$.

Based on these results, Mg is apparently a good candidate for an electron injecting contact in fullerene based devices. With appropriate contacts, it can be possible to determine accurate charge carrier mobilities without the need to correct for contact resistances. In practice, however, using Mg for the source and drain contacts for a systematic study is problematic due to its instability. Depositing a second contact over as a protective layer can lead to a slight mismatch between the contacts, altering the channel length and changing the injection conditions. Developing the Mg contacts further is a topic that warrants further investigations.

PCBM OFETs with Au contacts were found to deliver mobilities in the high $10^{-3}\text{cm}^2/\text{Vs}$ range according to equation (4.3), as were Al contacts. Once the effects of contact resistance had been taken into account, however, for the devices

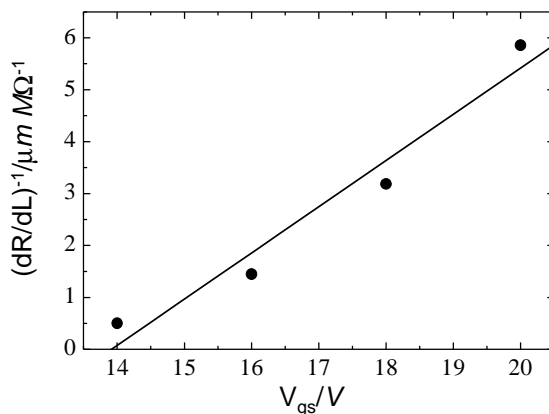


Figure 4.8: Channel resistance per unit length versus V_{gs} characteristics of a top contact PCBM (partner laboratory) OFET with Au source and drain contacts. The mobility was determined to be $2.6 \times 10^{-2} \text{cm}^2/\text{Vs}$ from the slope of the graph.

with Au contacts, the mobilities were found to be $2.6 \times 10^{-2} \text{cm}^2/\text{Vs}$. Figure 4.8 shows the channel resistance per unit length versus V_{gs} characteristics according to equation (4.12). The mobility was determined from the slope of the graph according to equation (4.12).

The mobilities from the devices with Al contacts did not increase after the effects of contact resistances were taken into account [123]. Values remained in the high $10^{-3} \text{cm}^2/\text{Vs}$ range. This is attributed to the differences in the injection processes and interface conditions between the various metals and the semiconductor. It is known that using a bilayer between the Al contact and semiconductor significantly improves electron injection [74; 107] in OLEDs, although the injection barrier for electrons is expected to be minimal between Al and the LUMO levels of many organic materials. Reactions between the metal contact and semiconductor can lead to significantly higher barriers than expected [76]. Charge injection processes into organic materials are not very well understood, and distinguishing between the dominant injection processes in a device can be challenging based on current-voltage measurements alone. As the mobilities are charge carrier density dependent, less efficient contacts may lead to lower charge carrier densities at a

given voltage, and hence lower mobilities. This may not necessarily be an effect that can be corrected for by examining the contact resistance, as only the losses directly at the metal-semiconductor interface are corrected for. In this regard, microscopic measurements on charge injection into OFETs, such as [69] and [65], where the voltage drop across the metal-semiconductor interface is directly measured, with spatial resolution, can potentially offer a lot of valuable information on the injection processes into organic semiconductors.

No evidence of hole mobilities was observed in the PCBM OFETs.

4.6.3 Temperature dependent current-voltage characteristics

The temperature dependent IV characteristics and electron field effect mobilities were investigated with the model introduced in section 4.4. The temperature dependent experimental data were fit according to equation (4.9) and the three material parameters, σ_o , α^{-1} , and T_{DOS} , were determined.

The I_{ds} versus V_{gs} characteristics of a bottom contact PCBM OFET with gold source and drain contacts are shown in figure 4.9 (open symbols). The PCBM investigated in the temperature dependent studies was purchased from Nano-C. The source-drain voltage was kept constant at 10V while the gate voltage was varied. The channel length of the sample was $80\mu\text{m}$, and the channel width 3mm. The measurements were taken in 10K steps between 190-290K.

The measured data were fit for each temperature. The data simulated from the fit results are shown in figure 4.9 (solid lines) for temperatures 290K, 250K, 220K and 190K. Only four temperature scans are shown here for clarity. The relative dielectric constant of the semiconductor, ϵ_r , was taken to be 3.9 for PCBM [127].

The parameters from the fit are summarised in table 4.1.

For all temperatures, at lower gate voltages, there is a discrepancy between experimental values and those predicted by the model. The experimental curves are slightly S shaped in comparison to the theoretical ones, resulting in lower currents. This is attributed to contact resistances resulting in a voltage drop across the channel, and resulting in a lower effective V_{ds} . This is pronounced at

4.6 Modelling charge transport in fullerene OFETs

Parameter	Value	Units
T_{DOS}	572	K
σ_o	2.44×10^{-5}	$\text{AV}^{-1}\text{m}^{-1}$
α^{-1}	4.18×10^{-10}	m^{-1}

Table 4.1: Parameters determined by modelling the transfer characteristics of a PCBM OFET over various temperatures: σ_o is the prefactor for the conductivity, α^{-1} is a factor representing the overlap between energy sites, and T_{DOS} signifies the width of the distribution of the exponential DOS

lower V_{gs} due to the gate voltage dependence of the contact resistance. According to equation (4.13) the contact resistance varies inversely with the electric field.

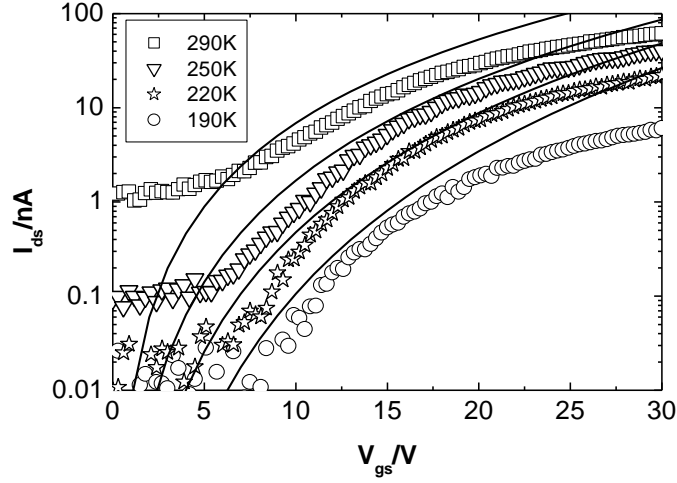


Figure 4.9: Experimental (symbols) and simulated (solid lines) I_{ds} versus V_{gs} characteristics of a bottom contact PCBM (Nano-C) OFET with Au source and drain contacts for various temperatures.

Interestingly, at lower and at higher temperatures, there was a large discrepancy observed between the predicted and experimentally determined values of I_{ds} . This may be expected at lower temperatures, as the contact resistance increases with decreasing temperature. At higher temperatures, however, the contact re-

sistance should be comparably smaller. This behaviour may be attributed to the contact resistances as the voltage drop at higher temperatures due to the contact resistance is more substantial due to the higher currents at higher temperatures, although it is not entirely clear why the current should saturate at higher temperatures. Room temperature measurements before and after the temperature scan delivered the same IV characteristics, which excludes the possibility of device degradation during the scan. The effects of the contact resistance are discussed in more detail later in the section.

4.6.4 Material parameters: comparison with values in the literature

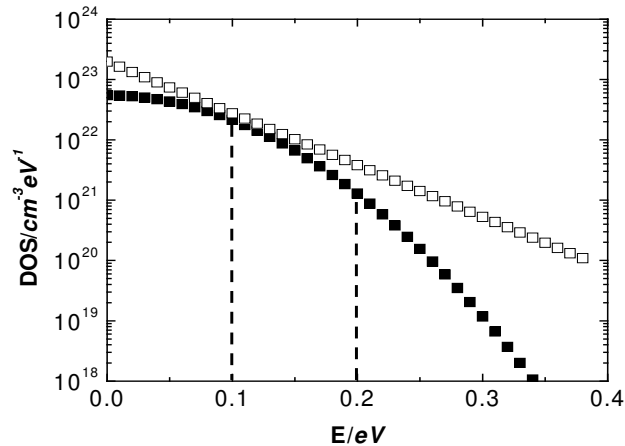


Figure 4.10: Comparison of the Gaussian DOS with a distribution width of $\sigma = 0.073\text{eV}$ (solid symbols) with an exponential DOS with a distribution width of $T_{DOS} = 572\text{K}$ (open symbols).

A study of PCBM diodes by Mihailetchi et al. [127] yielded that the electron transport in the methanofullerene could be described based on a correlated Gaussian disordered system. The width of the Gaussian DOS was found to be $\sigma = 0.073\text{eV}$ and the intersite spacing $a = 3.4\text{nm}$.

4.6 Modelling charge transport in fullerene OFETs

It was already mentioned in section 4.4 that an exponential DOS with an appropriate value of T_{DOS} can approximate a Gaussian DOS with a width of σ [102] over the energy range in which an OFET operates. Figure 4.10 shows the density of states versus energy for the Gaussian DOS with $\sigma = 0.073\text{eV}$ (closed symbols) and the exponential DOS with $T_{DOS} = 572\text{K}$ (open symbols).

The energy regime in which the OFET operates was determined from the activation energies of the field effect mobilities of the PCBM OFET. The field effect mobilities are discussed in more detail in the next section. The OFET was found to operate roughly between 0.1eV and 0.2eV. At $V_{gs} = 5\text{V}$, $E_a = 0.21\text{eV}$ and at $V_{gs} = 20\text{V}$ $E_a = 0.14\text{eV}$. From the figure it is apparent that in this energy range the exponential DOS with $T_{DOS} = 572\text{K}$ from the fit of the PCBM OFET IV characteristics is a good approximation for the Gaussian DOS with the value of $\sigma = 0.073\text{eV}$ found in [127].

4.6.5 Temperature dependent field effect mobilities

The electron field effect mobilities were determined according to equation (4.3) from the experimental I_{ds} versus V_{gs} data at temperatures from 190K to 300K. The mobility values determined then were fit according to equation (4.10) with the values for the parameters σ_o , α^{-1} , and T_{DOS} found in section 4.6.3. The measured (symbols) and simulated (solid lines) data are shown in figure 4.11.

As observed for the IV characteristics, at lower gate voltages the experimental values for the field effect mobility were found to be slightly lower than values predicted by the model. This can be seen in the figure, as the experimental mobilities at $V_{gs} = 10\text{V}$ are lower than the simulated values. At higher gate voltages, $V_{gs} = 15\text{V}$, the agreement is much better due to reduced effect of contact resistances at higher fields. The effect of contact resistances are considered in more detail in the next section.

The mobility demonstrates an Arrhenius type behaviour, as can be seen in figure 4.11. It can also be seen that the activation energy of the mobility depends on the applied gate voltage, which is consistent with the field dependent behaviour of μ_{FE} observed in organic semiconductors. Arrhenius plots for μ_{FE} determined

4.6 Modelling charge transport in fullerene OFETs

at several different gate voltages revealed that the mobility prefactor, μ_o , varies with the activation energy according to the Meyer-Neldel rule (equation (4.6)).

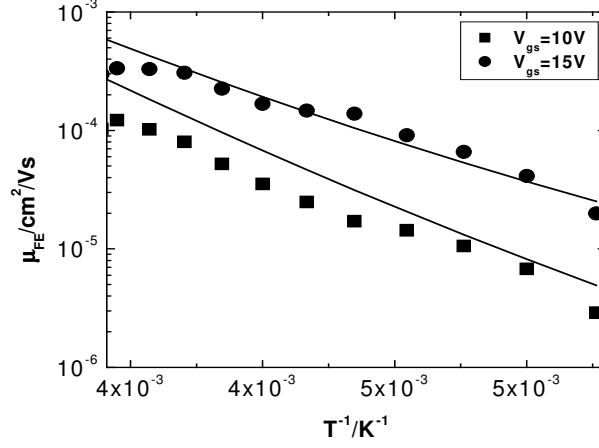


Figure 4.11: Arrhenius plots of the experimentally determined μ_{FE} of a bottom contact PCBM (Nano-C) OFET with Au source and drain contacts (symbols) and the simulated μ_{FE} values (lines) for $V_{gs} = 10V$ and $V_{gs} = 15V$.

Assuming $T_o = T_{DOS}$, μ_{oo} was found to be $3.6 \times 10^{-3} \text{cm}^2/\text{Vs}$. This value is lower than the room temperature mobility values found in 4.6.2. Although the discrepancy can be partially attributed to contact resistances in the bottom contact devices investigated here, the OFETs made with the commercially purchased PCBM showed consistently lower mobilities in various studies (by roughly a factor of 5, even after corrections for contact effects) than the PCBM acquired from the partner laboratory although the processing conditions were the same.

4.6.6 Correction due to the effects of contact resistances

4.6.6.1 Modelling the temperature and field dependence of the contact resistance

The effect of the contact resistance in bottom contact PCBM OFETs was investigated to understand the discrepancy, specifically at lower gate voltages, between

4.6 Modelling charge transport in fullerene OFETs

the experimental IV and μ_{FE} values and those predicted by the model. A contact resistance was calculated according to equation (4.14), with $T_o = T_{DOS}$ and $F = V_{gs}/t$ where t is the thickness of the gate insulator:

$$R_{con} = \frac{R_{oo}t}{V_{gs}} \exp\left(E_a \left[\frac{1}{k_B T} - \frac{1}{k_B T_{DOS}} \right]\right) \exp\left(\frac{(\phi_B - \Delta\phi)}{k_B T}\right).$$

The activation energy, E_a , the effective injection barrier, $\exp\left(\frac{(\phi_B - \Delta\phi)}{k_B T}\right)$, and the values of the contact resistance for several gate voltages at room temperature were determined first and the constant R_{oo} was then calculated afterwards.

It was already mentioned that the contact resistance has been observed to be activated with the same energy, E_a , as the field effect mobility [71]. The value of the activation energies from $V_{gs} = 0 - 30V$ were determined from field effect mobility.

The LUMO level of PCBM is given to be around 3.9eV in the literature. The work function of gold is given to be anywhere between 4.7 and 5.1eV. Once in contact with the PCBM layer, however, the effective work function is found to be typically higher due to interface effects. An effective barrier height for charge injection from Au into PCBM of 0.8 eV was assumed, which agrees with data from PCBM diodes with gold contacts [128]. There are two points to note here about the effective barrier for injection. Firstly, the value assumed for ϕ_B was found to only affect the magnitude of the constant R_{oo} , and not the shapes of the $R_{con}(T, V_{gs})$ versus V_{gs} curves. Secondly, based on the geometry of the bottom contact OFET, charges are injected from the source contact perpendicular to the electric field from the gate voltage [97]. The Schottky barrier lowering term is dependent on the field directly at the contact. Therefore, it was assumed that for a constant V_{ds} and varying V_{gs} , the effective barrier for injection remains constant.

The contact resistance was determined following the analysis outlined in section 4.5. The channel lengths were varied between several samples and the total device resistance was determined from the devices at various gate voltages. Device resistance was plotted against channel length for the different gate voltages (not shown here for brevity). The contact resistances were determined from the

4.6 Modelling charge transport in fullerene OFETs

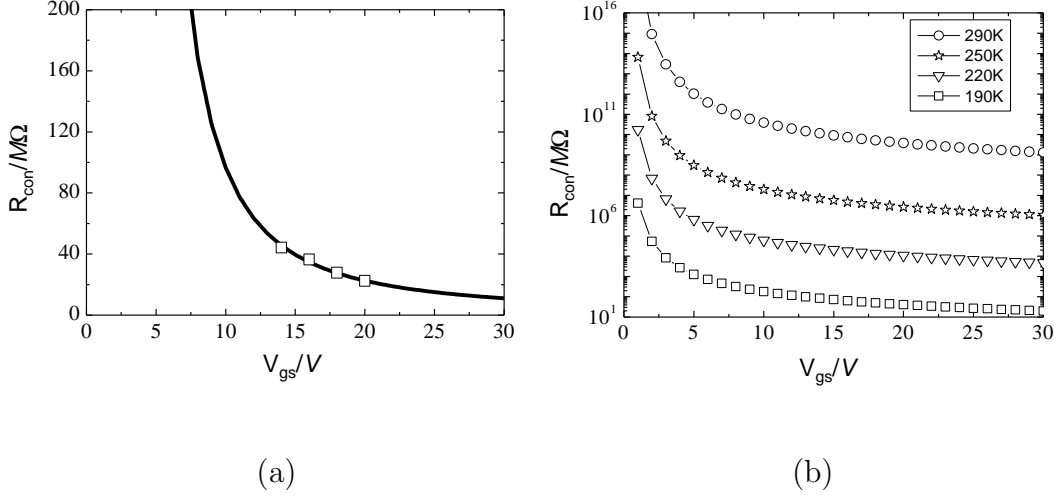


Figure 4.12: R_{con} versus V_{gs} : a) shows the experimentally determined (open symbols) for R_{con} and the simulated (solid line) values for room temperature and b) shows the simulated values for R_{con} for temperatures 290K, 250K, 220K, and 190K in semilogarithmic form for clarity.

y-intercepts of the plots. Values for the contact resistances were found to be in the order of $40M\Omega$ at a 14V gate voltage, and in the order of $20M\Omega$ at a gate voltage of 20V at room temperature. At lower gate voltages, currents were too low to make reliable measurements for the I_{ds} versus V_{ds} scans.

$R_{oo} = 380\Omega$ was then determined based on these results according to equation (4.14).

Figure 4.12 a) shows a plot of the experimental (open symbols) and simulated values (solid lines) for R_{con} versus the gate voltage at room temperature. It can be seen that there is good agreement between the few measured points and the simulated values. The proposed form for the contact resistance is based on the premise that the dominant injection processes in these devices is described by the DLTE model described in sections 3.3.2 and 3.3.2. This is strongly suggested by the inverse dependence of the contact resistance on the electric field and the charge carrier mobility, indicating that the injection current is also field and mobility dependent, consistent with a DTLE injection current [65; 69; 71].

For the expression of the contact resistance proposed here the disorder of the

4.6 Modelling charge transport in fullerene OFETs

system is considered, ie the observed Meyer-Neldel behaviour of the field effect mobility and hence of the contact resistance is accounted for, a phenomenon which is attributed to charge transport in a disordered system. The additional exponential term in the expression for the contact resistance due to the MN behaviour results experimentally in what would appear to be a smaller effective barrier for charge carrier injection when the DTLE model is strictly applied with no consideration of the system disorder. In microscopic studies of contact limited OFETs, the DLTE injection model was found to predict injection barriers that were larger than those measured experimentally [65; 69]. In [69] it is also suggested that accounting for the σ/kT term due to the Gaussian DOS could reduce the effective injection barrier height. Figure 4.12 b) shows the simulated values for R_{con} versus V_{gs} for temperatures 290K, 250K, 220K, and 190K. Figure 4.12 b) is shown in semilogarithmic form for clarity.

4.6.6.2 Correction to the simulated current-voltage data

The contact resistance results in a voltage drop in the areas around the source and drain contacts. This results in an effective voltage drop across the channel. The field and temperature contact resistance was incorporated into the model, and resulted in equation (4.9) becoming

$$I_{dsR} = \frac{WV_{ds} - I_{ds}R_{con}(V_{gs}T)\epsilon_o\epsilon_r\sigma_o}{Lq} \left(\frac{T}{2T_{DOS} - T} \right) \sqrt{\frac{2k_B T_{DOS}}{\epsilon_o\epsilon_r}} \times$$

$$\left(\frac{\left(\frac{T_{DOS}}{T}\right)^4 \sin\left(\pi\frac{T}{T_{DOS}}\right)}{(2\alpha)^3 B_c} \right)^{\frac{T_{DOS}}{T}} \left(\sqrt{\frac{\epsilon_o\epsilon_r}{2k_B T_{DOS}}} \left[\frac{C_i(V_{gs})}{\epsilon_o\epsilon_r} \right] \right)^{\frac{2T_{DOS}}{T} - 1},$$

where I_{ds} represents the initial values for the source-drain current calculated in section 4.6.3.

Figure 4.13 shows simulated and experimental I_{ds} versus V_{gs} characteristics. Open symbols represent the experimental data, the solid line represents the initial simulated data, and the dashed line represents the simulated data once the voltage drop due to contact resistance has been accounted for. Apparent is that there

4.6 Modelling charge transport in fullerene OFETs

is far better agreement between the experimental and simulated data once the contact resistances have been considered. Currents at lower gate voltages are better described, and the agreement between experimental and simulated data for temperatures 190K and 290K is improved. Discrepancies still exist at higher gate voltages. These are attributed to other effects. The thin semiconducting

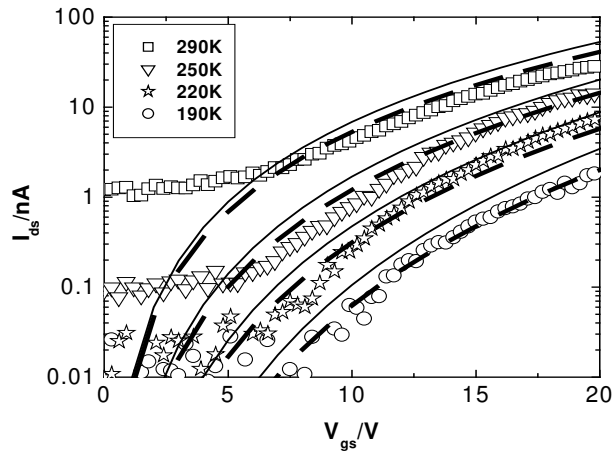


Figure 4.13: Temperature dependent I_{ds} vs V_{gs} characteristics of a bottom contact PCBM (Nano-C) OFET with Au source and drain contacts. The symbols show the experimental data, solid lines show the predicted values without considering the effects of the contact resistance, and the dashed lines show the predicted characteristics when the contact resistance has been considered.

films are not that robust against high gate voltages. Eventually the electric field due to the gate voltage is too high, and leakage currents through the insulator arise, lowering the channel current. This effect can be minimized by a better gate insulator and semiconductor-insulator interface. It is known that the quality of the gate insulator and the condition of the organic layer at the semiconductor-insulator interface has a strong effect on the performance of OFETs [129].

4.6.6.3 Correction to the simulated field effect mobility data

The calculated drop in V_{ds} was then incorporated into equation (4.10) for the case of the field effect mobility. Figure 4.14 shows the field effect mobilities once

the voltage drop across the channel has been accounted for. Only one voltage is shown here for clarity. Again, there is better agreement between simulated and experimental data at lower gate voltages.

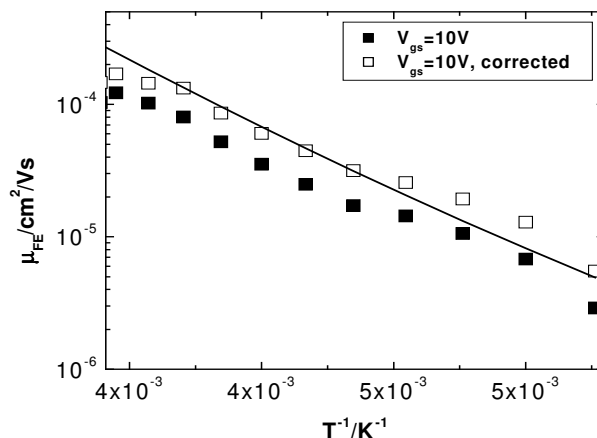


Figure 4.14: Temperature dependent mobilities determined of a bottom contact PCBM (Nano-C) OFET with Au source and drain contacts at $V_{gs} = 10\text{V}$. The closed symbols show the experimental data with a constant V_{ds} , and the open symbols show the experimental data once the voltage drop due to the contact resistance has been considered. The solid lines show the simulated data.

4.7 Summary

In this chapter, the charge transport in fullerene OFETs was investigated. A theoretical model for the field effect behaviour in organic semiconductors, developed in [110], was investigated in combination with the effects of contact resistances.

Charge transport in the fullerene derivative PCBM was investigated. Room temperature measurements of the field effect mobility demonstrated high mobilities ($2.2 - 2.6 \times 10^{-2} \text{cm}^2/\text{Vs}$). A comparison of the mobility values determined from devices with different metals used for the source and drain contacts revealed that Mg resulted in the best electron injection conditions, an effect which was attributed either to the doping of the fullerene layer by the Mg atoms, or the

formation of a MgO bilayer between the contact and semiconductor. Mobilities from PCBM OFETs with Au source and drain contacts also resulted in mobilities in the order of $10^{-2}\text{cm}^2/\text{Vs}$ once the effects of the contact resistances had been accounted for. The devices with Al source and drain contacts showed slightly lower mobilities, which could not be corrected upwards once contact effects had been considered. This is attributed to the domination of other injection processes in these devices.

The temperature dependent IV characteristics and field effect mobilities of a contact limited bottom contact PCBM OFET were then investigated in context of a model for the field effect characteristics of amorphous organic semiconductors [110]. An initial fit, without consideration of contact effects, led to values for the three material parameters σ_o , α^{-1} , and T_{DOS} . The distribution of the exponential DOS found in this study was found to agree well in the energy range in which the OFET operates with the distribution of the Gaussian DOS from a study on PCBM diodes found in the literature [127]. Discrepancies between the experimental data and values simulated from the model for I_{ds} and μ_{FE} at lower V_{gs} and temperatures were attributed to contact resistances.

An expression for the contact resistance was proposed. Simulated values for the contact resistance were calculated based on a DLTE injection current, room temperature values of the contact resistance, and accounting for the disorder in the system according to the Meyer-Neldel rule. Incorporating the voltage drop across the channel due to the contact resistance into the initial model resulted in a better agreement between the experimental and simulated values for the channel current and field effect mobility. These results confirm that the model in [110] is successful in describing the field effect behaviour of a variety of materials, from small molecules (pentacene), polymers (PPV and P3HT) [99; 110], to fullerenes, demonstrated here. In addition, through the contact resistance, information about the injection processes in OFETs is offered. Based on these results the injection currents in the PCBM OFETs can be described by a DTLE process with an effective injection barrier height lowered by disorder effects in the organic semiconductor.

Chapter 5

Organic photovoltaics: improving blend morphology in polymer-fullerene solar cells

5.1 Organic photovoltaics

5.1.1 History and development of organic solar cells

As in other areas of electronics, in the field of photovoltaics organic semiconductors have the potential to become a very cost effective alternative to the currently used materials. The production of photovoltaics from monocrystalline and polycrystalline silicon are very expensive, making the price of conventional silicon photovoltaics too outrageous for broad use or large scale applications. The cost for silicon photovoltaics is around $\$4/W$ and is estimated to level off within the next decade at best in the range of $\$1 - 1.50/W$, which is still far above the target price for photovoltaics (for a good review of the economic stand point of photovoltaics see [130]). Other materials have been investigated in order to avoid the use of the expensive silicon substrates and lower the cost of solar cell production [131]. The low cost and low energy input needed to fabricate organic solar cells is particularly attractive in the energy sector. With lower processing costs, lower power conversion efficiencies suffice to make the materials economically viable. The goal of reel to reel processing and printing techniques [132] with no high energy steps involved makes organic materials a serious candidate for photovoltaic applications.

In addition, organic solar cells can potentially be prepared on any type of substrate, allowing for flexible applications. The colour of the absorber layer and thin film structure allows for interesting possibilities that can be incorporated into the design and architecture of buildings, as incident light will pass through the device. An absorber layer used as window tint could serve as shading as well as an additional energy source for buildings. Doping, and the synthesis of new materials with different band gaps can lead to a wide colour variation in the cells. This is a fact, together with the light weight, that makes organic photovoltaic materials good candidates for portable electronics [133] or e-textiles [134].

Although organic semiconductors have relatively low charge carrier mobilities, they have fairly strong absorption coefficients [135], which leads to high absorption even for the thin absorber layers used. The success of OLEDs has contributed to the advances in organic photovoltaics, as many materials have already been screened and investigated.

Efficiencies reported for organic solar cells have been steadily increasing, as new suitable semiconducting materials are synthesised and investigated and device architectures improved. The first organic solar cells consisted of single layers of organic semiconductors sandwiched between contacts, and efficiencies reached 0.7% [136; 137] for vacuum deposited merocyanine dyes in these simple structures. Solar cells with two semiconducting components to form a heterojunction bilayer [138] or tandem structures [139] led to even higher efficiencies. For a good overview, see [135].

Polymer photovoltaics became a focus of research after the discovery of conducting polymers and the continued developments made in this field. The single polymer layer device architectures yielded very low efficiencies and high recombination effects which led to the motivation to introduce an electron acceptor into the system [140]. The use of an acceptor material can lead to a long lived charge separation state so that charge carriers can be collected at the device contacts before they recombine. A breakthrough came with the discovery of the ultra-fast charge transfer, which was reversible and metastable, between a conjugated polymer and a fullerene [140; 141]. This led to the development of the polymer-fullerene solar cell. The original bilayer cells [138] consisted of the polymer donor and fullerene acceptor separated by a single interface and had power

5.1 Organic photovoltaics

conversion efficiencies of 2%. Combining the polymer and fullerene components in a bulk-heterojunction structure to maximize contact between the polymer and fullerene, effectively creating a large number of donor-acceptor interfaces, led to much higher efficiencies. Power conversion efficiencies of these cells have been steadily increasing over the last few years [142; 143; 144; 145]. Solar cells made from the polymer poly(3-hexylthiophene) (P3HT), have exhibited efficiencies of 3.5% [144].

In this chapter the bulk-heterojunction polymer-fullerene solar cells with P3HT as the donor polymer and PCBM as the electron acceptor are the point of focus. The basic structure of the bulk heterojunction polymer-fullerene solar cell is shown in figure 5.1 along with the chemical structures of P3HT (upper left) and PCBM (lower left). A semitransparent contact sputtered onto a glass substrate serves as the anode. The blended layer of conjugated polymer-fullerene is applied to the substrate, typically by spin coating or doctor blading. The electrode is then applied on the semiconducting layer by means of vacuum deposition.

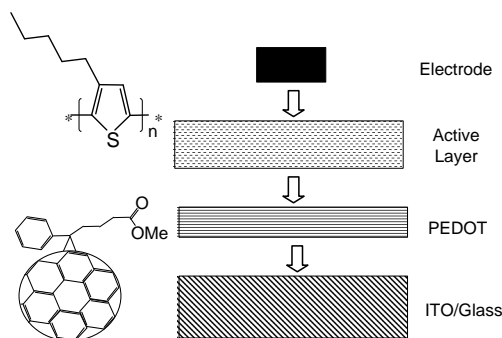


Figure 5.1: Left: chemical structures of P3HT (upper) and PCBM (lower). Right: structure of a polymer:fullerene bulk heterojunction solar cell.

The charge carrier mobilities in the polymer-fullerene blends are investigated for various PCBM contents. In addition the effect of tempering on the charge carrier mobilities is investigated.

5.1.2 Feasibility of organic solar cells

Organic solar cells must meet certain criteria before they can be introduced onto the market. Brabec et al. [146] recently examined the feasibility of commercial organic solar cells. Based on low cost production, the qualifications for market entry would be an efficiency of 5%, a lifetime of 3-5 years (correspondingly an operational lifetime of 3000-5000 hours). The introduction of printing techniques have the potential to considerably lower the cost of production to under 1US\$/W [146]. The efficiencies of these devices has been increasing steadily since the appearance of the first single layer polymer solar cell, and optimistically device efficiencies might be expected to continue to increase with the increasing understanding of the mechanisms behind these devices. The stability of the materials remains a question. Organic materials are sensitive to oxygen, water, sunlight, and temperature. Much research is needed in exploring means to protect and prolong the endurance of these devices.

5.2 Principals behind the polymer solar cell

The physics of organic semiconductors are much different under illumination than in the dark. In OLEDs and OFETs, the charges are injected from a contact, transported through the bulk, and then extracted at the other contact. The largest issues for charge transport are losses at the contacts (ie during charge injection or extraction due to interfaces traps, recombination, large interface barriers) and losses in the bulk due to chemical defects, unintentional doping, or poor film morphology, all which can result in traps for charge carriers.

The solar cell under illumination is quite a different case: the optically driven charge transfer between the polymer and fullerene, and the nature of the generated exciton within the bulk are specific to the solar cell. The charge carriers are excited within the bulk due to incident light. The charge transfer that occurs between the polymer and fullerene results in an electrically neutral and mobile (Frenkel) exciton with a relatively high binding energy [147]. Internal fields are too weak to dissociate the exciton; dissociation can occur at an interface between the donor and acceptor or at traps, where one charge carrier is trapped and the

5.2 Principals behind the polymer solar cell

other is free [147]. Ideally, the separated carriers are then extracted by an applied field and selective contacts before they can recombine.

Ideally, the hole and electron mobilities within a polymer solar cell should be balanced. Differing mobilities result in differing mean free paths of the individual charge carriers, which can lead to imbalanced distribution of charges within the semiconducting layer, whereby the slowest charges will determine the device performance [148]. The build up of one type of charge carrier within the bulk will lead to an electric field in the device opposing the flow of charge [149].

Generally the current in a solar cell can be described by

$$I = I_o \left(\exp \left[\frac{q}{nk_B T} (V - IR_s) \right] - 1 \right) + \frac{V - IR_s}{R_{sh}} - I_p, \quad (5.1)$$

where I_o is the dark current, n is the ideality factor of the diode, R_s is the series resistance, R_{sh} is the shunt resistance, and I_p is the photocurrent.

The efficiency of the device is then given by

$$\eta = \frac{FF I_{sc} V_{oc}}{P_{in}}. \quad (5.2)$$

V_{oc} is the open circuit voltage, I_{sc} is the short circuit current, and FF is the fill factor of the device, given by $FF = \frac{V_{MPP} I_{MPP}}{V_{oc} I_{sc}}$ where V_{MPP} , I_{MPP} are the voltage and current values taken at the maximum power point of the device, respectively.

It can then be seen that the efficiencies of these devices are directly dependent on the device parameters, such as the open circuit voltage (V_{oc}), the short circuit current (I_{sc}), and the fill factor [135].

The understanding as well as the isolation of the the electrical losses at the metal contacts and semiconductor interface [150; 151] due to recombination or large extraction barriers, or within the bulk of the device [148; 152; 153] resulting in charge carrier trapping or recombination are necessary to improve device efficiencies. Specifically, the current is determined by the wavelength region in which the semiconductor can absorb light, and by the morphology of the active layer. Poor morphology results in generally poor transport through the film. The current is also reduced by the recombination dynamics of charge carriers within

5.2 Principals behind the polymer solar cell

the bulk. The work functions of the contacts and the energetics of the donor and acceptor are factors that influence the open circuit voltage of the device.

In the next section we investigate the influence of the contacts and the semiconductor energetics on V_{oc} . After that, morphology effects on device performance are then discussed.

5.2.1 The open-circuit voltage

As already discussed in section 2.2.2, in the MIM picture, a built-in field results when an insulator is sandwiched between two contacts with asymmetric work functions. For a single component organic solar cell, the V_{oc} is then decided by the difference in the work functions of the two contacts or the Schottky barrier formation between the metal and doped organic layer [39]. In the case of single component organic photovoltaic devices, the V_{bi} in a device can then be easily determined as it is equal to the V_{oc} when the device is under (sufficiently strong) illumination [154].

In the case of more complicated donor-acceptor system, the work functions of the metals have again been observed to influence V_{oc} . The V_{oc} has also been shown to scale linearly with the difference between the metal work functions [155], and the use of Li:F as a bilayer for electron injection has been observed to increase the open-circuit voltage [143; 156]. Another study complimented these results by showing that changes to the work function of the electrode results in changes to the V_{oc} [157].

Other studies, however, have shown that the open-circuit voltage in the cell is determined by the energetics of the donor-acceptor system, ie V_{oc} is given by the difference between the HOMO of the donor and the LUMO of the acceptor. It was observed that the open-circuit voltage depends on the acceptor strength [158]. It was proposed that for ohmic contacts, the open-circuit voltage is determined by the energetics of the donor-acceptor system, while for non-ohmic contacts, the V_{oc} is limited by the difference in the work functions of the contacts [159]. Figure 5.2 demonstrates the two scenarios that can give rise to the open-circuit voltage.

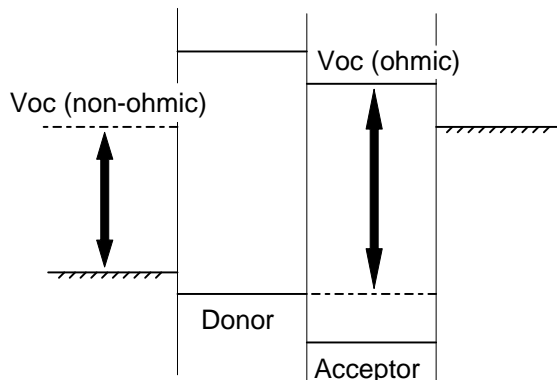


Figure 5.2: For ohmic contacts, the open circuit voltage is given by the difference in energy between the HOMO of the donor and the LUMO of the acceptor. For non-ohmic contacts, the V_{oc} is given by the difference in energy between the work functions of the device contacts.

5.2.2 The effect of morphology in polymer solar cells

The quality of the film morphology of donor-acceptor bulk heterojunction system is an extremely important for charge transport through the device. The morphology of the film depends on the solvent used, the method and conditions concerning the application of the solution to the substrate, the donor and acceptor being used, the concentration and ratio of donor and acceptor in the blend, and any post treatment, such as tempering, done to the device.

The principle of the bulk heterojunction structure is based on increased contact between the donor and acceptor in the blend. Studies on donor-acceptor systems on the same molecule [160; 161], however led to low efficiencies, attributed to the increased chance for recombination. Optimising the morphology is then perhaps a question of finding a compromise between reducing the charge carrier recombination with some phase separation between the donor and acceptor, and keeping the phase separation minimal enough to allow for the dissociation of excitons in the blend.

Studies on MDMO-PPV:PCBM [142] have shown that the solvent used can

impact device efficiencies. The most efficient devices reported were made with chlorobenzene as the solvent and a 80% PCBM content by weight. Measurements on PPV:PCBM blends via atomic force microscopy (AFM) and transmission electron microscopy (TEM) showed that phase separation in these blends (chlorobenzene) already begins to occur between 50% and 67% PCBM content by weight [162]. Measurements of the field effect mobilities of electrons and holes in the blends revealed that the electron and hole mobilities are balanced at the 80% PCBM weight content [163].

The higher hole mobilities in P3HT makes it an attractive for polymer photo-voltaics. Tempering, or heat treatment, is known to be essential for P3HT based devices, such as OLEDs [164], OFETs [10], and solar cells [144; 165; 166]. Heat treating some spin coated organic semiconductor films can lead to a rearrangement or crystallization of the molecules and, in the case of spin coated blends, can be used to improve the morphology [167; 168]. In the case of P3HT, heat treatment has been found to lead to oxygen dedoping, improved interchain interactions [169], and to a reduction in the free volume and in the defects at the interface between contact and semiconductor due to evaporation of the solvent [164].

Until now, investigations of the effects of tempering have focused on changes in electric transport and optical properties relating to P3HT. In this chapter the effect of tempering on PCBM:P3HT blends is investigated and it is found that, in addition to improved hole mobilities, tempering drastically improves the electron mobilities within the blends.

5.3 Experimental

The field effect transistors were prepared using highly doped p-Si wafers as the gate electrode. A layer of thermally grown SiO₂ served as the gate insulator. All solutions were prepared with chloroform and applied to the wafer via spin coating. The source and drain electrodes were evaporated onto the semiconducting layer to produce top contact OFETs for these studies. Processing was done under a defined nitrogen atmosphere. Tempering was done at 110°C for 30s, unless otherwise specified in the text. Measurements were performed in vacuum and in

the dark. The P3HT investigated here is regioregular P3HT synthesized following the Rieke procedure [170] and was bought from Rieke Met. Inc. The synthesis of PCBM is the same as described in [121] and was acquired from the partner laboratory in Groningen.

5.3.1 Field effect mobilities in P3HT films

5.3.1.1 Tempering in P3HT films

Tempering leads to a slight increase in the field effect mobilities of holes in P3HT films. Figure 5.3 shows the I_{ds} versus V_{ds} scans for various gate voltages before and after tempering for a P3HT OFET. The hole mobilities were determined according to equation (4.3). Before tempering, hole mobilities were found to be 2.3×10^{-4} and after tempering, hole mobilities were found to be 4.0×10^{-4} . In addition to the increase in mobility, the leakage currents through the gate oxide were reduced due to tempering in some samples (not shown here).

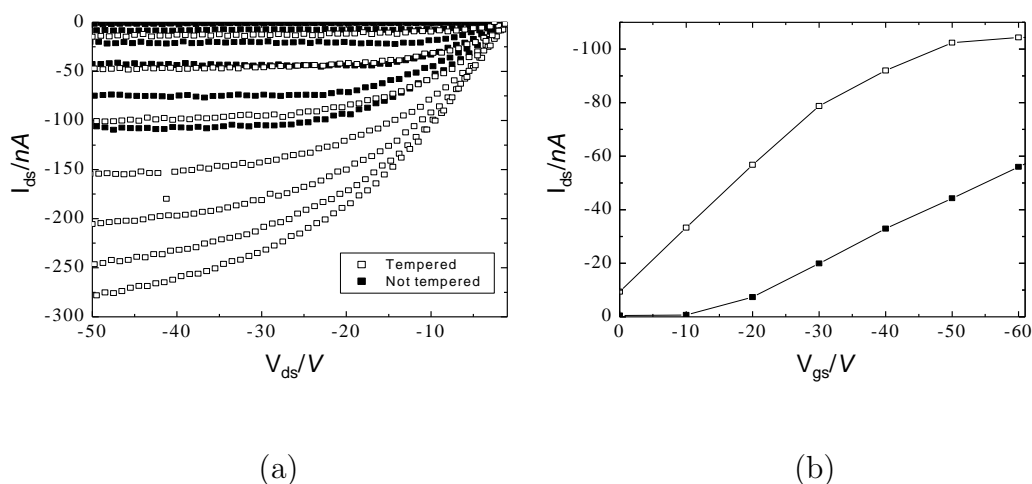


Figure 5.3: a) I_{ds} versus V_{gs} characteristics of a P3HT OFET for gate voltage values of $V_{gs} = 0 - 60V$ measured before and after tempering. Closed squares stand for the data before tempering, while open squares stand for data after tempering. b) I_{ds} vs V_{gs} characteristics for the same device before and after tempering.

5.3.1.2 Consideration of contact effects

It was already shown in the previous chapter that contact effects can influence the IV characteristics from OFETs. In the case of mobility measurements, contact resistances can lead to lower mobility measurements when not accounted for. Gold was used as for the source and drain electrodes in these devices. Although Au is assumed to form an ohmic contact with the HOMO level of P3HT, there are reports of non-ohmic injection from Au into P3HT diodes [171], and contact resistances have been previously reported for P3HT OFETs with Au contacts [71; 116]. It has also already been shown that the hole mobility estimation from P3HT OFETs with Au contacts increases by at least one order of magnitude when the contact resistances are considered according to equation (4.12) [71; 123].

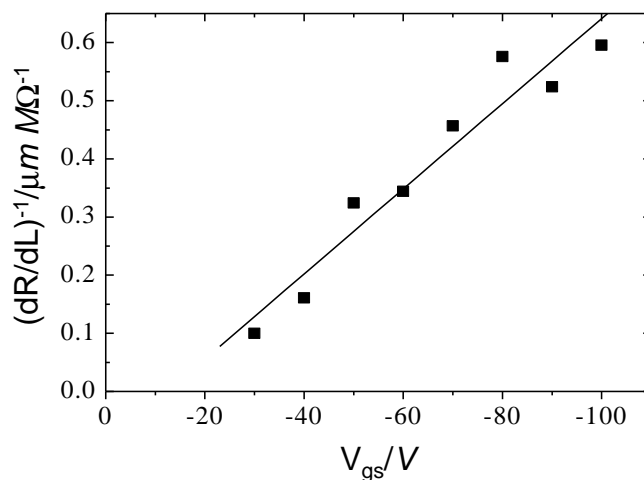


Figure 5.4: Channel resistance per unit length versus V_{gs} characteristics for a tempered P3HT OFET. A mobility of 2.8×10^{-3} was determined from the slope of the graph.

Hole mobilities in tempered P3HT films in the OFET structure with Au source-drain contacts determined according to (4.3)

$$\frac{\partial I_{ds}}{\partial V_{gs}} = \mu_{FE} W C_i V_{ds} / L$$

were found to be 4×10^{-4} . Accounting for the contact resistances, according to equation (4.12),

$$\frac{\partial[(\partial R_{tot}/\partial L)^{-1}]}{\partial V_{gs}} = \mu_{FE} W C_i$$

the hole mobilities are then found to be 2.8×10^{-3} . Figure 5.4 shows the I_{ds} versus V_{gs} characteristics, once contact resistances have been considered. Other metals were then investigated as source-drain contacts in an attempt to lower losses at the contacts (Cu, Ag), but the determined mobility values remained in the same order.

There was no observed evidence for electron transport in the P3HT devices.

5.3.2 The effect of tempering in the polymer-fullerene blends

5.3.2.1 Variation of PCBM content in the blend

The charge carrier mobilities in tempered and not tempered PCBM:P3HT blends were then investigated. Au was used for the source and drain contacts for all of the OFETs so that both charge carrier mobility types could be investigated in the same device with more predictable results. It was already shown in section 4.6.2 that once the effects of contact resistances had been corrected for, mobilities of $2.6 \times 10^{-2} \text{cm}^2/\text{Vs}$ in PCBM OFETs with Au source and drain contacts were determined.

The electron and hole mobilities in the blends were first investigated from the I_{ds} versus V_{gs} scans according to equation (4.3) without correcting for contact effects. Although the effects of the contact resistances were demonstrated to be

substantial in previous sections, the trend of the charge carrier mobilities in the blends for varying PCBM content is of interest here. For the sake of comparison, electron and hole mobilities at the same PCBM concentration were determined from the same device. The contact effects were then corrected for in the case of the optimal blend ratio by following the analysis outlined in section 4.5, where the device resistances of several OFETs with different channel lengths were measured to isolate the contact resistance and determine a more accurate mobility value.

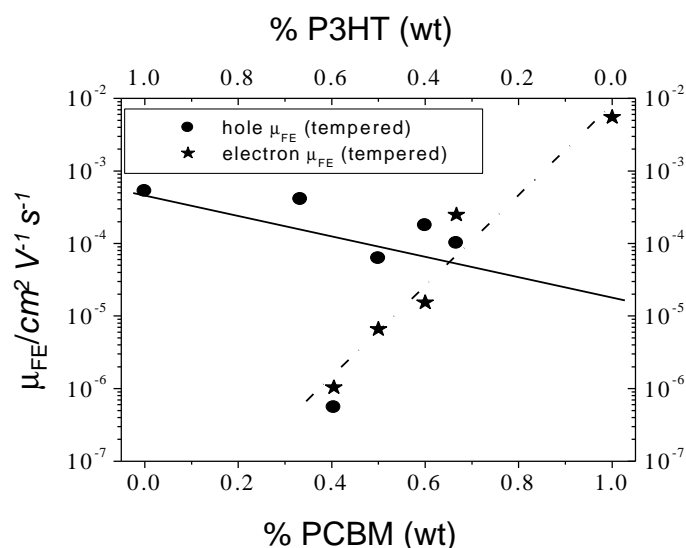


Figure 5.5: Electron and hole mobilities (not corrected for the effects of contact resistances) for various weight percentages of PCBM in tempered PCBM:P3HT blends. The concentration of P3HT was kept constant for all solutions, and electron and hole mobilities were measured from the same device. The mobilities of pure PCBM and pure, tempered P3HT are included for comparison.

The PCBM content was varied in the blend, and the charge carrier mobilities were determined. The amount of P3HT was kept constant (1 wt % in chloroform) for all blends, except for the case of pure PCBM. The amount of PCBM was then varied between the PCBM:P3HT blends: 0:1 (0% PCBM), 0.5:1(33%), 0.68:1(40%), 1:1 (50%), 1.5:1 (60%), 2:1 (67%) and 1:0 (100%). Figure 5.5 shows the change in the electron and hole mobilities in the blends for increasing PCBM

content, as well as the mobilities in pure P3HT and PCBM films (0% and 100%). For the sake of comparison, all mobilities at the same PCBM concentration were determined according to equation (4.3) from the same device.

The hole mobilities remain roughly constant in the $10^{-4}\text{cm}^2/\text{Vs}$ range, decreasing slightly for increasing PCBM content, with the exception of 40% PCBM content, which is understood to be an experimental artifact.

Apparent here is that the electron mobility increases with increasing PCBM content. For the 2:1 PCBM:P3HT ratio, the hole and electron mobilities are roughly balanced. Electron mobility was first visible in blends with weight ratios of 0.68:1 PCBM:P3HT (40% PCBM), and only in tempered blends. In blends that were not tempered, the electron mobilities were first apparent for 2:1 blends (67%). Only the charge carrier mobilities in tempered blends are shown here for clarity, and the lines between the data points are intended as guides for the eye. The solid lines show the trend of the hole mobilities, while the dashed line shows that of the electron mobilities. The effect of tempering on the charge carrier mobilities is investigated in the next section, and summarized in table 5.3.2.2, along with mobilities corrected for the effect of contact resistances.

5.3.2.2 The effect of tempering on electron transport in blends

The effect of tempering in pure P3HT films was investigated in an earlier section, and was found to lead to a slight increase in the field effect mobility by roughly a factor of 2. The effect of tempering was then investigated in pure PCBM films and on 2:1 PCBM:P3HT films.

In the pure PCBM films, tempering was found to have little effect. Short tempering at low temperatures (10s at 100°C) led to a reduction in the leakage currents, which is attributed to a better contact being made between metal and semiconductor. Longer tempering, however, led to device degradation.

The charge carrier mobilities were found to be balanced in the 2:1 PCBM:P3HT blends, and so the effect of tempering on the charge carrier mobilities was specifically investigated in these blends. An improvement in the hole mobility was not detected, although leakage currents were reduced. The hole mobility determined according to eq. (4.3) was found to be $1 \times 10^{-4}\text{cm}^2/\text{Vs}$ for both the not tempered and tempered cases. The mobility was found to be $8.5 \times 10^{-4}\text{cm}^2/\text{Vs}$, slightly

lower than the hole mobility in pure P3HT, for the tempered blends after the effect of contact resistances had been considered. Figure 5.6 shows the modified I_{ds} vs V_{gs} characteristics for the hole transport in a tempered 2:1 PCBM:P3HT blend.

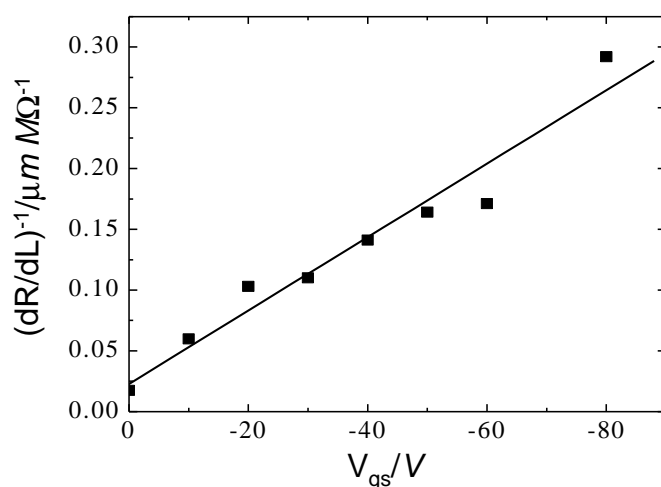


Figure 5.6: Channel resistance per unit length versus V_{gs} characteristics for hole transport in a tempered 2:1 PCBM:P3HT OFET. From the slope of the graph a mobility of $8.5 \times 10^{-4} \text{cm}^2/\text{Vs}$ could be determined.

In the case of electron mobilities in blends, the effect of tempering led to a strong increase in the electron mobility.

Figure 5.7 shows the I_{ds} versus V_{gs} characteristics for electron transport in a 2:1 PCBM:P3HT OFET before and after tempering for gate voltages between 0V and 50V. General IV characteristics improved due to tempering, and the mobility increased by nearly a factor of 10, from $7.0 \times 10^{-5} \text{cm}^2/\text{Vs}$ to $4.0 \times 10^{-4} \text{cm}^2/\text{Vs}$.

Figure 5.8 shows the resistance per unit length versus V_{gs} characteristics, according to eq. (4.12) for the electron mobilities in a tempered 2:1 PCBM:P3HT blend. From the slope, a mobility of low $10^{-3} \text{cm}^2/\text{Vs}$ was determined. This is lower than the mobility in pure PCBM, suggesting that the morphology may limit electron transport.

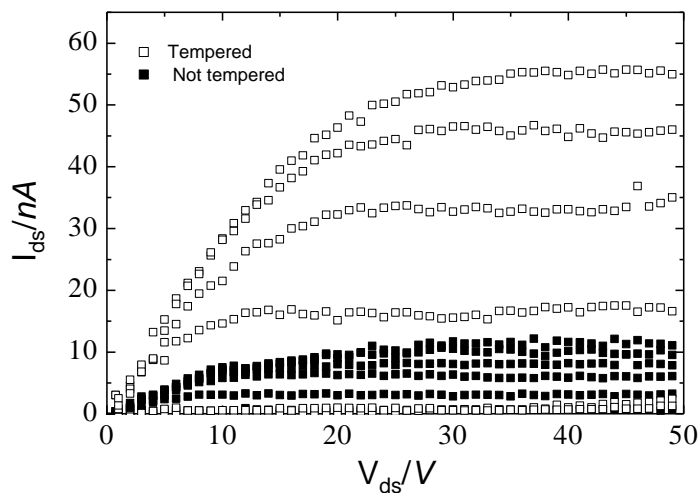


Figure 5.7: I_{ds} versus V_{ds} for gate voltages of $V_{gs} = 0 - 50\text{V}$ for electron transport in a PCBM:P3HT OFET measured before (closed symbols) and after (open symbols) tempering.

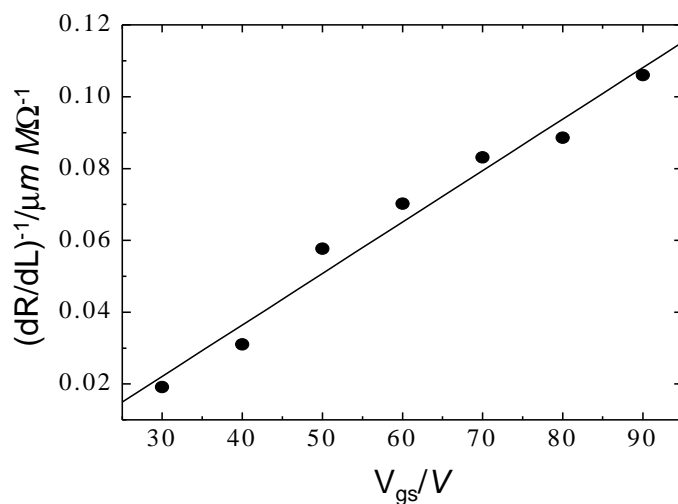


Figure 5.8: I_{ds} versus V_{gs} characteristics, corrected for contact resistances, for electron transport in a tempered 2:1 PCBM:P3HT blend OFET.

Table 5.3.2.2 summarizes the results for mobilities in not tempered and tempered films and blends, as well as the mobilities corrected for the effects of contact resistance.

Material	Before tempering cm ² /Vs	After tempering cm ² /Vs
P3HT (hole)	2.3×10^{-4}	4.0×10^{-4}
corrected	-	2.8×10^{-3}
PCBM (electron)	8.4×10^{-3}	5.5×10^{-4}
corrected	2.9×10^{-2}	-
PCBM/Mg (electron)	1.2×10^{-2}	-
2:1 PCBM:P3HT (hole)	1.0×10^{-4}	1.0×10^{-4}
corrected	-	8.5×10^{-4}
2:1 PCBM:P3HT (electron)	7.0×10^{-5}	4.0×10^{-4}
corrected	-	1.3×10^{-3}

Table 5.1: Charge carrier mobilities before and after tempering in films and blends.

5.4 Summary

It is known that the absorption spectrum of PCBM:P3HT blends made in chloroform changes in the wavelength regime attributed to P3HT due to heat treatment, while the spectra of pure P3HT and pure PCBM remain the same, and that tempering leads to phase separation and hence to the growth of PCBM clusters within the bulk due to structural modifications resulting in a more planar structure (the yellow to red phase transition) [165]. A slight increase was observed in the hole mobility in pure P3HT after tempering, while no change in the electron mobility in PCBM was detected. For the electron transport in blends, however, tempering appears to be crucial. In blends with lower PCBM content that were not tempered, no electron mobility is observed, and for blends with higher PCBM content an almost 10 fold increase in the electron mobility is observed after tempering.

Tempering the blend results in a change in the morphology of the bulk. Before tempering, electron transport sites are scattered throughout the bulk, isolated

from other sites by the polymer chains. The growth of PCBM clusters after tempering results in larger transport sites. When the PCBM content is high enough, these sites form a delocalized electron transport path through the bulk.

The morphology of the blend, although improved by tempering, remains an obstacle for efficient charge transport. Charge carrier mobilities in the blends are lower than in pure PCBM and P3HT. Hole mobilities in the blends decrease slowly for increasing PCBM. In comparison, electron mobilities rise rapidly with increasing PCBM content. At 2:1 PCBM:P3HT ratios, the mobilities are balanced in the low $10^{-3}\text{cm}^2/\text{Vs}$ range. Recently Chirvase et al. [165] reported that 1:1 PCBM:P3HT blends delivered the best solar cell parameters, and that at higher PCBM concentrations, PCBM clusters diffuse out of the polymer matrix and damage the semiconductor/metal interface. At this ratio, however, the electron mobilities are 10 times lower than the hole mobilities. To exclude the possibility that the tempering times were insufficient, these devices were retempered. This, however, led to a decrease in both electron and hole mobilities.

For polymer-fullerene solar cells, it seems that the damage to the contact as well as a decrease in the hole mobility in the blend at higher PCBM contents are more detrimental to the efficiency of the solar cell than the unbalanced charge carrier mobilities. The mobilities depend on the phase separation achieved in the blend, which determines the possible pathways between the donor and acceptor. In order to further improve solar cell efficiencies, it is necessary to first optimize the morphology of the blend. The solvent used as well as the tempering parameters will directly impact the morphology, and therefore also the mobility of the charge carriers in the bulk. This requires further investigations of the effect of different solvents and various tempering times and temperatures on the charge carrier mobilities as well as on the solar cell parameters.

Chapter 6

Conclusions

In this thesis, the electric transport properties of charge carriers in organic semiconductors were investigated. Energetic and positional disorder in the bulk means that energy sites are localised; and charge carriers are transported via electric field and temperature assisted hopping. Field effect measurements offer a good and direct method of investigating the transport properties of charge carriers through the semiconductor bulk by means of the field and temperature dependent field effect mobilities.

Fullerene OFETs were investigated here as little work has been done to date on n-type OFETs. The field effect mobilities in PCBM OFETs at room temperature were found to be in the order of $10^{-2}\text{cm}^2/\text{Vs}$, which relatively high for an organic semiconducting film. Good current-voltage characteristics were achieved with Mg source-drain contacts due to reduced contact resistances.

It was shown the the temperature dependent IV characteristics and field effect mobilities in PCBM OFETs could be well described by a previously proposed model based on hopping in an exponential density of states. The temperature dependence of the current-voltage characteristics and the field effect mobility could be modelled, and the results from the fit agreed with results from studies in the literature on PCBM diodes.

In addition to investigating the charge transport properties in the bulk of the semiconductor, it was shown that intentionally studying contact limited OFETs can offer information about the injection process from metal into organic material, as injection currents depend on the contact resistances between the metal and

semiconductor. The injection process into organic semiconductors is still largely not understood, and experimental work to isolate injection currents into organic devices is valuable. The contact resistances in OFETs demonstrate temperature and field dependence, and vary inversely with the mobility. This behaviour suggests injection currents that follow the diffusion limited thermionic emission model. Contact resistances were determined at room temperature, and in combination with the activation energy from the field effect mobility, the temperature dependence of the contact resistance could be modelled. Including the effects of the contact resistance in the model improved the agreement between the experimental data and data simulated from the model substantially.

In addition to investigating the transport properties of the individual materials, it is also possible to gain information about the quality of the semiconducting film for semiconductors produced in solution form and then applied to the substrate via spincoating, doctor blading, etc. In the final section of this thesis, materials commonly used in polymer-fullerene solar cells were investigated. The hole mobilities in pure P3HT, with consideration of the effects of tempering and also contact effects were investigated. Tempering led to an increase in the hole mobilities by roughly a factor of 2. Contact effects, even in devices assumed to have ohmic contacts, can be detrimental for mobility measurements. In the case of pure P3HT, contact effects reduce the determined hole mobilities by a factor of 10. Correcting led to mobilities in the $10^{-3}\text{cm}^2/\text{Vs}$ range. The field effect mobilities in polymer-fullerene blends were then investigated. Tempering was found to be crucial for the electron mobilities in the blends. Hole and electron mobilities were found to be balanced at $10^{-3}\text{cm}^2/\text{Vs}$ for a 2:1 PCBM:P3HT blend composition, once the contact resistances had been considered.

Chapter 7

Appendix A: Experimental Setup

7.1 General

An experimental setup for the measurement of organic field effect transistors was designed and constructed as a part of this thesis. Measurements were performed inside of a cryostat, in the dark. All measurements were computer automated: a LabView program controlled the instruments via a GPIB interface. The cold finger from the cryostat had a total of 18 connections leading from the bottom, where the sample holder is located, to the top where the cold finger is attached to the cryostat. Half of terminals were needed for the temperature controller: PT-100 sensor (4-point) and heater resistance. The other half were used for the current-voltage measurements. Three contacts are needed for each OFET, and the nine contacts allowed for the flexibility of contacting multiple devices on a single sample from outside the cryostat, without exposing the sample to air.

7.2 Samples

OFETs were prepared on highly doped (p++ for n-type and n++ for p-type OFETs) silicon wafers, cut into square samples with dimensions $15 \times 15 \text{ mm}^2$. A layer of thermally grown SiO_2 served as the gate dielectric. The SiO_2 layer had

a thickness of 100-300 nm. The wafers were ordered processed and precut from the company Microfab.

The source and drain contacts were deposited onto the samples in a vacuum chamber under high vacuum. A shadow mask was used to structure the source and drain contacts on the substrate. Two shadow masks were used to pattern the source-drain contacts and samples were prepared with either 3 rows of 4 OFETs, each with a width of 2mm, or 3 rows with 1 OFET, each with a width of 4mm. The 12 OFET samples were used for determining contact resistance due to the higher comparability of devices fabricated under the same conditions. The samples with the 3 devices delivered higher currents due to the wider channels, and were used for temperature dependent measurements. Channel lengths in both cases were in the range of 20 – 200 μm . Figure 7.1 shows the structure of one of the 12 OFET samples.

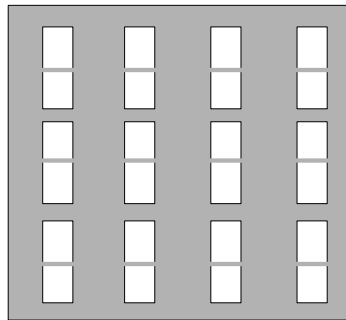


Figure 7.1: A sample with 12 OFETs.

7.3 Sample holder

The sample holder was attached to the end of a cool finger which is inserted into the cryostat. The sample holder was plated with copper and gold to improve thermal conductivity. The sample fit into a small indent in the sample holder, as shown in figure 7.2, and the back of the sample holder served as the gate contact,

and was grounded. This allowed for the best thermal coupling to the sample. A contact bridge with 2x4 spring contacts allowed for possibility of contacting of 4 transistors on the sample simultaneously. This reduces the amount of air that the sample is exposed to, as the individual transistors on the sample could be contacted from outside the cryostat once the sample was already in the cryostat under vacuum.

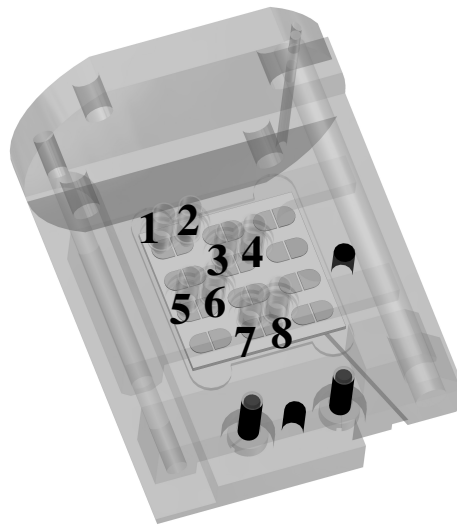


Figure 7.2: Diagram of the sample holder for OFET measurements. 12 spring contacts on a mobile contact bridge allow for the contacting of four OFETs simultaneously.

7.4 Current-voltage sweep

OFETs are three terminal devices. The typical configuration is: the source contact is grounded, and a voltage between the gate and source contacts is applied

7.5 Temperature dependent measurements

resulting in an accumulation of charge in the semiconducting layer. A voltage applied between the source and drain contacts will result in a flow of charge across the source-drain channel. In this setup, however, due to the better thermal coupling mentioned above, the gate contact was grounded, and voltages were directly applied between the source and gate contacts and between the drain and gate contacts. Only the potential difference between the terminals is important for the measurements. The source, drain and gate voltages were then calculated accordingly for data analysis. One source-measurement-unit (SMU) was used to supply the voltage between the source and gate voltage (Keithley 6517), and another source-measurement unit (SMU) was used to perform the source-drain current-voltage sweep (Keithley 236).

The setup also allows for the measurement of diodes when a simple current-voltage sweep is performed. It can be expanded for solar cell measurements if a light source is incorporated.

7.5 Temperature dependent measurements

A Lakeshore 330 temperature controller was used for the temperature scans. A PT-100 inside the sample holder was used for temperature measurements. A heater resistance controlled by the LS 330, and also inside the sample holder, was used for counter heating. A constant flow of liquid nitrogen was used for cooling during the temperature scans.

Bibliography

- [1] M. Pope and C. E. Swenberg, *Electronic Processes in Organic Crystals and Polymers*, University Press, Oxford, second edition, 1999. [1.1](#), [1.2](#), [1.2](#), [3.1](#)
- [2] H. Shirakawa, E. J. Louis, A. G. MacDiarmid, C. K. Chiang, and A. J. Heeger, *J. Chem. Soc. Chem. Comm.* , 579 (1977). [1.1](#), [1.2](#)
- [3] G. Hadziioannou and P. van Hutten, editors, *Semiconducting polymers: chemistry, physics, engineering*, Wiley-VCH, Weinheim, 1999. [1.2](#)
- [4] R. A. Janssen, L. Smilowitz, N. S. Sariciftci, and D. Moses, *J. Chem. Phys.* **101**, 1787 (1994). [1.2](#)
- [5] G. Horowitz, *Adv. Mater.* **10**, 365 (1998). [1.2](#), [4.2](#), [4.2.1](#), [4.2.1](#), [4.3](#), [4.3.2](#)
- [7] P. W. M. Blom, M. J. M. de Jong, and M. G. van Munster, *Phys. Rev. B* **55**, R656 (1997). [1.2](#)
- [8] E. Cantatore, ESSDERC **invited paper** (2001). [1.2](#)
- [6] R. J. O. M. Hoofman, *Nature* **392**, 54 (1998). [1.2](#)
- [11] A. Salleo, T. W. Chen, A. R. Völkel, Y. Wu, P. Liu, B. S. Ong, and R. A. Street, *Phys. Rev. B* **70**, 115311 (2004). [1.2](#)
- [9] H. Sirringhaus, P. J. Brown, R. H. Friend, M. M. Nielsen, K. Bechgaard, B. M. W. Lanveld-Voss, A. J. H. Spiering, R. A. J. Janssen, E. W. Meijer, P. Herwig, and D. M. de Leeuw, *Nature* **401**, 685 (1999). [1.2](#)

- [10] G. Wang, J. Swensen, D. Moses, and A. J. Heeger, *J. Appl. Phys.* **93**, 6137 (2003). [1.2](#), [5.2.2](#)
- [12] E. M. Conwell, *Phys. Rev.* **103**, 51 (1956). [1.3](#)
- [13] N. F. Mott, *Canadian J. Phys.* **34**, 1356 (1956). [1.3](#)
- [15] H. Bässler, *phys. stat. sol (b)* **175**, 15 (1993). [1.3](#), [1.3](#), [4.4](#)
- [14] A. Miller and E. Abrahams, *Phys. Rev* **120**, 745 (1960). [1.3](#)
- [16] M. Grunewald and P. Thomas, *phys. stat. sol. (b)* **94**, 125 (1979). [1.3](#)
- [18] D. Monroe, *Phys. Rev. Lett.* **54**, 146 (1985). [1.3](#)
- [17] F. R. Shapiro and D. Adler, *J. Non-Cryst. Solids* **74**, 189 (1985). [1.3](#)
- [19] V. I. Arkhipov, E. V. Emelianova, and H. Bässler, *Phil. Mag. B* **81**, 985 (1996). [1.3](#)
- [20] E. V. Emelianova and G. J. Adriaenssens, *J. Optoelectron. Adv. Mater.* **6**, 1105 (2004). [1.3](#), [3.1](#)
- [21] S. D. Baranovskii, T. Faber, F. Hensel, and P. Thomas, *J. Phys.: Condens. Matter* **9**, 2699 (1997). [1.3](#)
- [22] H. Andoniadis, M. A. Abkowitz, and B. R. Hsieh, *Appl. Phys. Lett.* **65**, 2030 (1994). [1.3](#)
- [23] S. A. Choulis, Y. Kim, J. Nelson, D. D. C. Bradley, M. Giles, M. Shkunov, and I. McCulloch, *Appl. Phys. Lett.* **85**, 3890 (2004). [1.3](#)
- [24] C. W. Tang and S. A. VanSlyke, *Appl. Phys. Lett.* **51**, 913 (1987). [2.1](#)
- [25] J. H. Burroughes, D. D. C. Bradley, A. R. Brown, R. N. Marks, K. Makay, R. Friend, P. L. Burns, and A. B. Holmes, *Nature* **347**, 539 (1989). [2.1](#)
- [27] S. A. Carter, M. Angelopoulos, S. Karg, P. J. Brock, and J. C. Scott, *Appl. Phys. Lett.* **70**, 2067 (1997). [2.1](#)

- [26] J. C. Scott, S. A. Carter, S. Karg, and M. Angelopoulos, *Synth. Met.* **85**, 1197 (1997). [2.1](#)
- [28] R. H. Friend, *Pure Appl. Chem.* **73**, 425 (2001). [2.1](#)
- [29] N. F. Mott and R. W. Gurney, *Electronic Processes in Ionic Crystals*, Oxford University Press, Oxford, second edition, 1948. [2.2](#), [2.2.1](#)
- [30] V. I. Arkhipov, P. Heremans, E. V. Emelianova, and G. J. Adriaenssens, *Appl. Phys. Lett.* **79**, 4154 (2001). [2.2](#)
- [31] M. A. Lampert and P. Mark, *Current injection in solids*, Academic Press, New York, 1970. [2.2.1](#)
- [32] P. N. Murgatroyd, *J. Phys. D: Appl. Phys.* **3**, 151 (1969). [2.2.1](#), [2.2.1](#)
- [35] P. W. M. Blom, M. J. M. de Jong, and J. J. M. Vleggaar, *Appl. Phys. Lett.* **68**, 3308 (1996). [2.2.1](#), [2.2.2.2](#)
- [33] S. Nešpůrek and J. Sworakowski, *J. Appl. Phys.* **51**, 2098 (1980). [2.2.1](#)
- [34] F. Schauer, S. Nešpůrek, and H. Valerián, *J. Appl. Phys.* **80**, 880 (1996). [2.2.1](#)
- [36] A. Kadashchuck, Y. Skryshevskii, A. Vakhnin, N. Ostapenko, V. I. Arkhipov, E. Emilianova, and H. Bässler, *Phys. Rev. B* **63**, 115205 (2001). [2.2.2.1](#)
- [37] H. Frohne, D. C. Müller, and K. Meerholz, *ChemPhysChem* **8**, 707 (2002). [2.2.2.2](#)
- [38] F. Cacialli, R. H. Friend, N. Haylett, R. Daik, W. J. Feast, D. A. dos Santos, and J. L. Brédas, *Appl. Phys. Lett.* **69**, 3794 (1996). [2.2.2.2](#)
- [39] S. M. Sze, editor, *Physics of Semiconductor Devices*, John Wiley and Sons, New York, 1981. [2.2.2.3](#), [5.2.1](#)
- [41] T. M. Brown, J. S. Kim, R. H. Friend, F. Cacialli, R. Daik, and W. J. Feast, *Appl. Phys. Lett.* **75**, 1679 (1999). [2.2.2.3](#)

- [40] G. G. Malliaras, J. R. Salem, P. J. Brock, and C. Scott, Phys. Rev. B **58**, R13411 (1998). 2.2.2.3
- [42] B. Bohnenbuck, Charge transport in organic diodes, Master's thesis. 2.3, 2.3
- [44] H. Ishii, K. Sugiyama, E. Ito, and K. Seki, Adv. Mater. **11**, 605 (1999). 3.1
- [43] S. Narioka, H. Ishii, D. Yoshimura, M. Sei, Y. Ouchi, K. Seki, S. Hasegawa, T. Miyazaki, Y. Harima, and K. Yamashita, Appl. Phys. Lett. **67**, 1899 (1995). 3.1
- [46] R. Schlaf, P. G. Schroeder, M. W. Nelson, B. A. Parkinson, P. A. Lee, K. W. Nebesny, and N. R. Armstrong, J. Appl. Phys. **86**, 1499 (1999). 3.1
- [45] T. Shimada, K. Hamaguchi, A. Koma, and F. S. Ohuchi, Appl. Phys. Lett. **72**, 1869 (1998). 3.1
- [47] J. M. Barathan and Y. Yang, J. Appl. Phys. **84**, 3207 (1998). 3.1
- [48] O. W. Richardson, *The Emission of Electricity from Hot Bodies*, Longmans Green and Company, London, 1921. 3.2
- [49] W. Schottky, Z. Physik. **15**, 872 (1914). 3.2
- [50] R. H. Fowler and L. Nordheim, Proc. Roy. Soc. **121**, 626 (1928). 3.2
- [52] Z. Chiguvare, J. Parisi, and V. Dyakonov, J. Appl. Phys. **94**, 2440 (2003). 3.2
- [51] I. D. Parker, J. Appl. Phys. **75**, 1658 (1995). 3.2
- [53] P. S. Davids, S. M. Kogan, I. D. Parker, and D. L. Smith, J. Appl. Phys. **69**, 2270 (1996). 3.2
- [54] J. G. Simmons, Phys. Rev. Lett. **15**, 967 (1965). 3.2, 3.3.2
- [55] P. R. Emtage and J. J. O'Dwyer, Phys. Rev. Lett. **16**, 365 (1965). 3.2, 3.3.2

- [56] M. A. Baldo and S. R. Forrest, Phys. Rev. B. **64**, 085201 (2000). [3.2](#)
- [57] Y. Shen, W. Klein, D. B. Jacobs, J. C. Scott, and G. G. Malliaras, Phys. Rev. Lett. **86**, 3867 (2001). [3.2](#), [4.5](#)
- [58] M. A. Abkowitz, H. A. Mizes, and J. S. Facci, Appl. Phys. Lett. **66**, 1288 (1995). [3.2](#)
- [59] E. M. Conwell and M. W. Wu, Appl. Phys. Lett. **70**, 1867 (1997). [3.2](#)
- [60] V. I. Arkhipov, E. V. Emelianova, Y. H. Tak, and H. Bässler, J. Appl. Phys. **84**, 848 (1998). [3.2](#), [3.3.2](#)
- [61] U. Wolf, V. I. Arkhipov, and H. Bässler, Phys. Rev. B **59**, 7507 (1999). [3.2](#)
- [62] V. I. Arkhipov, U. Wolf, and H. Bässler, Phys. Rev. B **59**, 7514 (1999). [3.2](#)
- [63] S. Barth, U. Wolf, H. Bässler, P. Müller, H. Riel, H. Westweber, P. F. Seidler, and W. Rieß, Phys. Rev. B **60**, 8791 (1999). [3.2](#)
- [64] J. C. Scott and G. G. Malliaras, Chem. Phys. Lett **299**, 115 (1999). [3.2](#), [3.3.2](#)
- [65] W. R. Silveira and J. A. Marohn, Phys. Rev. Lett. **93**, 116104 (2004). [3.2](#), [3.3.2](#), [4.5](#), [4.5](#), [4.5](#), [4.6.2](#), [4.6.6.1](#)
- [66] M. A. Abkowitz and D. M. Pai, Philos. Mag. B **53**, 193 (1986). [3.3.1](#)
- [67] M. A. Abkowitz, J. S. Facci, and M. Stolka, Appl. Phys. Lett. **63**, 1892 (1993). [3.3.1](#)
- [68] A. Ioannidis, M. A. Abkowitz, and J. S. Facci, J. Appl. Phys. **84**, 1439 (1998). [3.3.1](#)
- [69] L. Bürgi, T. J. Richards, R. H. Friend, and H. Sirringhaus, J. Appl. Phys. **94**, 6129 (2003). [3.3.2](#), [3.3.2](#), [4.5](#), [4.5](#), [4.5](#), [4.6.2](#), [4.6.6.1](#)

- [70] R. J. Chesterfield, J. C. McKeen, C. R. Newman, C. D. Frisbie, P. C. Ewbank, K. R. Mann, and L. L. Miller, *J. Appl. Phys.* **95**, 6396 (2004). [3.3.2](#), [4.5](#), [4.5](#)
- [71] B. H. Hamadani and D. Natelson, *Appl. Phys. Lett.* **84**, 443 (2004). [3.3.2](#), [4.5](#), [4.5](#), [4.6.6.1](#), [4.6.6.1](#), [5.3.1.2](#)
- [72] T. van Woudenberg, P. W. M. Blom, M. C. J. M. Vissenberg, and J. N. Huiberts, *Appl. Phys. Lett.* **79**, 1697 (2001). [3.3.2](#)
- [73] C. R. Newman, C. D. Frisbie, D. A. da Silva Filho, J. L. Brédas, P. C. Ewbank, and K. R. Mann, *Chem. Mater.* **16**, 4436 (2004). [3.3.3](#)
- [74] L. S. Hung, C. W. Tang, and M. G. Madson, *Appl. Phys. Lett.* **70**, 152 (1996). [3.3.3](#), [4.6.2](#)
- [76] R. H. Friend, R. W. Gymer, A. B. Holmes, J. H. Burroughs, R. N. Marks, C. Taliani, D. D. C. Bradley, D. A. D. Santos, J. L. Brédas, and M. Lögdlund and W R Salaneck, *Nature* **397**, 121 (1999). [3.3.3](#), [4.6.2](#), [4.6.2](#)
- [75] Y. Gao, K. T. Park, and B. R. Hsieh, *J. Appl. Phys.* **73**, 7894 (1993). [3.3.3](#), [4.6.2](#)
- [77] A. V. Slyke, C. H. Chen, and C. W. Tang, *Appl. Phys. Lett.* **69**, 2160 (1996). [3.3.3](#)
- [78] D. Kahng and M. M. Atalla, IRE Solid-State Devices Research Conference, Carnegie Institute of Technology, Pittsburg, PA (1960). [4.1](#)
- [79] D. F. Barbe and C. R. Westgate, *J. Phys. Chem. Solids* **31**, 2679 (1970). [4.1](#)
- [80] M. L. Petrova and L. D. Rozenshtein, *Fiz. Tverd. Tela (Sov. Phys. - Solid State)* **12**, 961 (1970). [4.1](#)
- [81] H. Koezuka, A. Tsumura, and T. Ando, *Synth. Met.* **18**, 699 (1987). [4.1](#)
- [82] A. Dodabalapur, J. Laquindanum, H. E. Katz, and Z. Bao, *Appl. Phys. Lett.* **69**, 4227 (1996). [4.1](#)

- [83] Y. Y. Lin, A. Dodabalapur, R. Sarpeshkar, Z. Bao, W. Li, K. Baldwin, V. R. Raju, and H. E. Katz, *Appl. Phys. Lett.* **74**, 2714 (1999). 4.1
- [85] H. E. A. Huitema, G. H. Gelinck, J. B. P. H. van der Putten, K. E. Kuijk, C. Hart, E. Cantatore, P. T. Herwigm, A. J. J. M. van Breemen, and D. M. de Leeuw, *Nature* **414**, 599 (2001). 4.1
- [84] P. Mach, S. J. Rodriguez, R. Nortrup, P. Wiltzius, and J. A. Rogers, *Appl. Phys. Lett.* **78**, 3592 (2001). 4.1
- [86] B. K. Crone, A. Dodabalapur, A. Gelperin, L. Torsi, H. E. Katz, A. J. Ovinger, and Z. Bao, *Appl. Phys. Lett.* **78**, 2229 (2001). 4.1
- [87] C. J. Drury, C. M. J. Mutsaers, C. M. Hart, M. Matters, and D. M. de Leeuw, *Appl. Phys. Lett.* **73**, 108 (1998). 4.1
- [88] G. H. Gelinck, T. C. T. Geuns, and D. M. de Leeuw, *Appl. Phys. Lett.* **77**, 1487 (2000). 4.1
- [89] A. Hepp, H. Heil, W. Weise, M. Ahles, R. Schmechel, and H. von Seggern, *Phys. Rev. Lett.* **91**, 157406 (2003). 4.1
- [90] C. D. Dimitrakopoulos and P. R. L. Malenfant, *Adv. Mater.* **14**, 99 (2002). 4.1
- [91] Y. Sun, Y. Liu, and D. Zhu, *J. Mater. Chem.* **15**, 53 (2005). 4.1
- [92] R. W. I. de Boer, M. E. Gershenson, A. F. Morpurgo, and V. Podzorov, *phys. stat. sol. (a)* **6**, 1302 (2004). 4.1
- [93] V. C. Sundar, J. Zaumseil, V. Podzorov, E. Menard, R. L. Willett, T. Someya, M. E. Gershenson, and J. A. Rogers, *Science* **303**, 1644 (2004). 4.1
- [94] S. F. Nelson, Y. Y. Lin, D. J. Gundlach, and T. N. Jackson, *Appl. Phys. Lett.* **72**, 1854 (1998). 4.1
- [95] G. Horowitz, *Adv. Mater.* **13**, 53 (2003). 4.1

- [96] P. V. Necliudov, M. S. Shur, D. J. Grundlach, and T. N. Jackson, *J. Appl. Phys.* **88**, 6594 (2000). [4.3.1](#), [4.5](#)
- [97] R. A. Street and A. Salleo, *Appl. Phys. Lett.* **81**, 2887 (2002). [4.3.1](#), [4.5](#), [4.6.6.1](#)
- [98] G. Horowitz, R. Hajlaoui, H. Bouchriha, R. Bourguiga, and M. Hajlaoui, *Adv. Mater.* **10**, 923 (1998). [4.3.1](#)
- [99] E. J. Meijer, C. Tanase, P. W. M. Blom, E. van Veenendaal, B.-H. Huisman, D. M. de Leeuw, and T. M. Klapwijk, *Appl. Phys. Lett.* **80**, 3838 (2002). [4.3.1](#), [4.4](#), [4.4](#), [4.7](#)
- [100] E. J. Meijer, C. Detcheverry, P. J. Baesjou, E. V. Veenendaal, D. M. D. Leeuw, and T. M. Klapwijk, *J. Appl. Phys.* **98**, 4831 (2003). [4.3.1](#)
- [101] G. Horowitz, R. Hajlaoui, D. Fichou, and A. E. Kassmi, *J. Appl. Phys.* **85**, 3202 (1999). [4.3.2](#)
- [102] C. Tanase, E. J. Meijer, P. W. M. Blom, and D. M. de Leeuw, *Phys. Rev. Lett.* **91**, 216601 (2003). [4.3.2](#), [4.4](#), [4.6.4](#)
- [103] W. Meyer and H. Neldel, *Z. Tech. Phys.* **12**, 588 (1937). [4.3.3](#)
- [105] Y. F. Chen and S. F. Huang, *Phys. Rev. B* **44**, 13775 (1991). [4.3.3](#)
- [104] R. S. Crandall, *Phys. Rev. B* **43**, 4057 (1991). [4.3.3](#)
- [106] W. B. Jackson, *Phys. Rev. B* **38**, 3595 (1998). [4.3.3](#)
- [108] A. Hamed, Y. Y. Sun, Y. K. Tao, R. L. Meng, and P. H. Hor, *Phys. Rev. B* **47**, 10873 (1993). [4.3.3](#)
- [107] J. C. Wang and Y. F. Chen, *Appl. Phys. Lett.* **73**, 948 (1998). [4.3.3](#), [4.6.2](#)
- [109] E. J. Meijer, , M. Matters, P. T. Herwig, D. M. D. Leeuw, and T. M. Klapwijk, *Appl. Phys. Lett.* **76**, 3433 (2000). [4.3.3](#)
- [110] M. C. J. M. Vissenberg and M. Matters, *Phys. Rev. B* **57**, 12 964 (1998). [4.4](#), [4.4](#), [4.4](#), [4.4](#), [4.4](#), [4.7](#)

- [111] G. E. Pike and C. H. Seager, Phys. Rev. B **10**, 1421 (1974). 4.4
- [112] S. Luan and G. W. Neudeck, J. Appl. Phys. **72**, 766 (1992). 4.5
- [113] E. von Hauff, J. Parisi, and V. Dyakonov, PRB **submitted** (2005). 4.5
- [114] K. Seshadri and C. D. Frisbie, Appl. Phys. Lett. **78**, 993 (2001). 4.5
- [116] L. Bürgi, H. Sirringhaus, and R. H. Friend, Appl. Phys. Lett. **80**, 2913 (2001). 4.5, 5.3.1.2
- [115] T. Hassenkam, D. R. Greve, and T. Bjornholm, Adv. Mater. **13**, 631 (2001). 4.5
- [117] V. Podzorov, V. M. Pudalov, and M. E. Gershenson, Appl. Phys. Lett. **82**, 1739 (2003). 4.5
- [118] D. M. de Leeuw, M. M. J. Simenon, A. R. Brown, and R. E. F. Einerhand, Synth. Met. **87**, 53 (1997). 4.6
- [119] H. W. Kroto, J. R. Heath, S. C. O'Brien, R. F. Curl, and R. E. Smalley, Nature **318**, 162 (1985). 4.6
- [120] L. Forró and L. Mihály, Rep. Prog. Phys. **64**, 649 (2001). 4.6
- [121] J. C. Hummelen, B. W. Knight, F. LePeq, F. Wudl, J. Yao, and C. L. Wilkins, J. Org. Chem. **60**, 532 (1995). 4.6, 5.3
- [123] E. von Hauff, V. Dyakonov, and J. Parisi, Sol. Energy Mater. Sol. Cells **87**, 149 (2005). 4.6.2, 4.6.2, 5.3.1.2
- [122] C. Waldauf, P. Schilinsky, M. Perisutti, J. Hauch, and C. J. Brabec, Adv. Mater. **15**, 2084 (2003). 4.6.2
- [124] E. J. Meijer, D. M. D. Leeuw, S. Setayesh, E. V. Veenendaal, B. H. Huisman, P. W. M. Blom, J. C. Hummelen, U. Scherf, and T. M. Klapwijk, Nature Mater. **2**, 678 (2003). 4.6.2
- [125] V. D. Mihailetschi, P. W. M. Blom, J. C. Hummelen, and M. T. Rispen, J. Appl. Phys. **94**, 6849 (2003). 4.6.2

- [126] M. Chikamatsu, S. Nagamatsu, T. Taima, Y. Yoshida, N. Sakai, H. Yokokawa, K. Saito, and K. Yase, *Appl. Phys. Lett.* **85**, 2396 (2004). [4.6.2](#)
- [127] V. D. Mihailetschi, J. K. J. van Duren, P. W. M. Blom, J. C. Hummelen, R. A. J. Janssen, J. M. Kroon, M. T. Rispens, W. J. H. Verhees, and M. M. Wienk, *Adv. Funct. Mater.* **13**, 43 (2003). [4.6.3](#), [4.6.4](#), [4.7](#)
- [128] J. K. J. van Duren, V. D. Mihailetschi, P. W. M. Blom, T. van Woudenberg, J. C. Hummelen, R. A. J. Janssen, and M. M. Wienk, *J. Appl. Phys.* **94**, 4477 (2003). [4.6.6.1](#)
- [129] H. Sirringhaus, N. Tessler, and R. H. Friend, *Science* **280**, 1741 (1998). [4.6.6.2](#)
- [130] S. Shaheen, D. S. Ginley, and G. E. Jabbour, *MRS Bulletin* **30**, 10 (2005). [5.1.1](#)
- [131] K. Zwiebel, B. von Roedern, and H. Ullal, *Photon Int.* , 48 (2004). [5.1.1](#)
- [132] S. E. Shaheen, R. Radspinner, N. Peyghambarian, and G. E. Jabbour, *Appl. Phys. Lett.* **79**, 2996 (2001). [5.1.1](#)
- [133] J. M. Shaw and P. F. Seidler, *IBM J. Res. & Dev.* **45**, 3 (2001). [5.1.1](#)
- [134] S. Wagner, E. Bonderover, W. B. Jordan, and J. C. Sturm, *IJHSES* **12**, 391 (2002). [5.1.1](#)
- [135] H. Hoppe and N. S. Sariciftci, *J. Mater. Res.* **19**, 1924 (2004). [5.1.1](#), [5.2](#)
- [137] A. K. Gosh and T. Feng, *J. Appl. Phys.* **49**, 5982 (1978). [5.1.1](#)
- [136] D. L. Morel, A. K. Gosh, T. Feng, E. L. Stogryn, P. E. Purwin, R. F. Shaw, and C. Fishman, *Appl. Phys. Lett* **32**, 495 (1978). [5.1.1](#)
- [138] C. W. Tang, *Appl. Phys. Lett.* **48**, 183 (1986). [5.1.1](#)
- [139] M. Hiramoto, M. Suezaki, and M. Yokoyama, *Chem. Lett.* **19**, 327 (1990). [5.1.1](#)

BIBLIOGRAPHY

- [140] N. S. Saraciftci, L. Smilowitz, A. J. Heeger, and F. Wudl, *Science* **258**, 1474 (1992). [5.1.1](#)
- [141] L. Smilowitz, N. S. Saraciftci, R. Wu, C. Gettinger, A. J. Heeger, and F. Wudl, *Phys. Rev. B* **48**, 15425 (1993). [5.1.1](#)
- [143] C. J. Brabec, S. E. Shaheen, C. Winder, N. S. Sariciftci, and P. Denk, *Appl. Phys. Lett.* **80**, 1288 (2002). [5.1.1](#), [5.2.1](#)
- [145] C. J. Brabec, V. Dyakonov, J. Parisi, and N. S. Sariciftci, editors, *Organic Photovoltaics*, Springer, Berlin, 2003. [5.1.1](#)
- [144] F. Padinger, R. Rittberger, and N. S. Sariciftci, *Adv. Funct. Mater.* **13**, 1 (2003). [5.1.1](#), [5.2.2](#)
- [142] S. E. Shaheen, C. J. Brabec, N. S. Sariciftci, F. Padinger, T. Fromherz, and J. C. Hummelen, *Appl. Phys. Lett.* **78**, 15 (2001). [5.1.1](#), [5.2.2](#)
- [146] C. J. Brabec, J. A. Hauch, P. Schilinsky, and C. Waldauf, *MRS Bulletin* **30**, 50 (2005). [5.1.2](#)
- [147] B. A. Gregg and M. C. Hanna, *J. Appl. Phys.* **93**, 3605 (2002). [5.2](#)
- [148] D. Gebeyehu, C. J. Brabec, F. Padinger, T. Fromherz, J. C. Hummelen, D. Badt, H. Schindler, and N. S. Sariciftci, *Synth. Met.* **118**, 1 (2000). [5.2](#), [5.2](#)
- [149] A. C. Arango, L. R. Johnson, V. N. Bliznyuk, Z. Schlesinger, S. A. Carter, and H.-H. Hörhold, *Adv. Mater.* **12**, 1689 (2000). [5.2](#)
- [151] J. Gao, H. Wang, and F. Hide, *Synth. Met.* **84**, 979 (1997). [5.2](#)
- [150] G. Yu, J. Gao, J. C. Hummelen, F. Wudl, and A. J. Heeger, *Science* **270**, 1789 (1995). [5.2](#)
- [152] W. U. Huynh, J. J. Dittmer, N. Teclerian, D. J. Milliron, and A. P. Alivisatos, *Phys. Rev. B* **67**, 115326 (2003). [5.2](#)

- [153] I. Riedel, J. Parisi, V. Dyakonov, L. Lutsen, D. Vanderzande, and J. C. Hummelen, *Adv. Funct. Mater.* **14**, 38 (2004). [5.2](#)
- [154] G. G. Malliaras, J. R. Salem, P. J. Brock, and J. C. Scott, *J. Appl. Phys.* **84**, 1583 (1998). [5.2.1](#)
- [155] J. Liu, Y. Shi, and Y. Yang, *Adv. Funct. Mater.* **11**, 420 (2001). [5.2.1](#)
- [156] F. L. Zhang, M. Johansson, M. R. Anderson, J. C. Hummelen, and O. Inganäs, *Synth. Met.* **137**, 1401 (2003). [5.2.1](#)
- [157] H. F. S. E. Shaheen, C. J. Brabec, D. C. Müller, N. S. Saraciftci, and K. Meerholz, *ChemPhysChem* **3**, 795 (2002). [5.2.1](#)
- [158] C. J. Brabec, A. Cravino, D. Meissner, N. S. Sariciftci, T. Fromherz, M. T. Rispens, L. Sanchez, and J. C. Hummelen, *Adv. Funct. Mater.* **11**, 374 (2001). [5.2.1](#)
- [159] V. D. Mihailetschi, P. W. M. Blom, J. C. Hummelen, and M. T. Rispens, *J. Appl. Phys.* **94**, 6849 (2003). [5.2.1](#)
- [160] J.-F. Ekert, J.-F. Nicoud, J.-F. Nierengarten, S.-G. Liu, L. Echegoyen, F. Barigelletti, N. Armaroli, L. Ouali, V. Krasnikov, and G. Hadziioannou, *J. Am. Chem. Soc.* **122**, 7467 (2000). [5.2.2](#)
- [161] F. Zhang, M. Svensson, M. R. Andersson, M. Maggini, S. Bucella, E. Menna, and O. Inganäs, *Adv. Mater.* **13**, 1871 (2001). [5.2.2](#)
- [162] J. K. J. van Duren, X. Yang, J. Loos, C. W. T. Bulle-Lieuwma, A. B. Sieval, J. C. Hummelen, and R. A. J. Janssen, *Adv. Funct. Mater.* **14**, 425 (2004). [5.2.2](#)
- [163] W. Geens, S. E. Shaheen, C. J. Brabec, J. Poortmans, and N. S. Saraciftci, 14th International Winterschool/Euroconference, Kirchberg, Austria (2000). [5.2.2](#)
- [164] T. Ahn, H. Lee, and S. Han, *Appl. Phys. Lett.* **80**, 392 (2002). [5.2.2](#)

BIBLIOGRAPHY

- [165] D. Chirvase, J. Parisi, J. C. Hummelen, and V. Dyakonov, *Nanotechnology* **15**, 1317 (2004). [5.2.2](#), [5.4](#)
- [166] I. Riedel and V. Dyakonov, *phys. stat. sol. (a)* **201**, 1332 (2004). [5.2.2](#)
- [167] J. J. Dittmer, E. A. Marseglia, and R. H. Friend, *Adv. Mater.* **12**, 1270 (2000). [5.2.2](#)
- [168] W. U. Huynh, J. J. Dittmer, W. C. Libby, G. L. Whitting, and A. P. Alivisatos, *Adv. Funct. Mater.* **13**, 73 (2003). [5.2.2](#)
- [169] P. J. Brown, D. S. Thomas, A. Köhler, J. Wilson, J.-S. Kim, C. M. Ramsdale, H. Sirringhaus, and R. H. Friend, *Phys. Rev. B* **67**, 064203 (2003). [5.2.2](#)
- [170] T.-A. Chen, X. Wu, and D. Rieke, *J. Am. Chem. Soc.* **117**, 223 (1995). [5.3](#)
- [171] D. B. A. Rep, A. F. Morpurgo, and T. M. Klapwijk, *Org. Electron.* **4**, 201 (2003). [5.3.1.2](#)

Acknowledgements

I would like to acknowledge the following people for their help and support for the duration of my thesis:

- Vladimir Dyakonov for offering me the opportunity to start this thesis and providing the continued motivation to complete it.
- Jürgen Parisi for his experience and the constant support which helped me to finish this thesis.
- My colleagues and fellow Phd students: Susanne Böger, Zivayi Chiguvare, Dana Chirvase, Martin Knipper, Verena Mertens, Michael Pientka and Ingo Riedel for their ideas, eagerness to help, and the time they took just to listen.
- Britta Bohnenbuck, my diploma student, for her dedication.
- The diploma students: Eva Schlenker, Martin Schreiner, and Johannes Sieger.
- Holger Koch for his ever ingenious ideas and the many hours he put in to ensure that OFETs could be measured at the Uni Oldenburg.
- Hans Holtorf, Tanja Schwanitz (Miesner), and Wilhelm Jürgens for their support.
- My many colleagues in the EHF, especially Achim Kittel who offered many a good idea during spontaneous hallway conversations, Macro Munzel, and Jens Reemts.
- My friends - Katharina for talking me through crises while running :- and family.
- Mike. For everything :)

CV

Elizabeth Leoni von Hauff

geboren am 20.09.1977 in York, Kanada

Berufstätigkeit

2002–2005: Wissenschaftliche Mitarbeiterin im Institut für Physik
an der Carl von Ossietzky Universität Oldenburg

2001–2002: Wissenschaftliche Mitarbeiterin in der Nachwuchsgruppe
Theoretische Biophysik an der
Friedrich-Schiller-Universität Jena

Akademische Ausbildung

2002–2005: Promotion an der Universität Oldenburg bei
Prof. V. Dyakonov

Thema: *“Field effect investigations of charge carrier
transport in organic semiconductors”*

2000–2001: *MSc Renewable Energy* an der Universität Oldenburg

Thema: *“Production and characterization of an
organic solar cell”*

1996–2000: *BSc Honours* in Physik, University of Alberta in
Edmonton, Kanada

Thema: *“Design and construction of a single shot
autocorrelator for an amplified ti:saph laser system”*

Schulbildung

1982–1995: Abschluss *Advanced High School Diploma*
in Edmonton, Kanada

Erklärung

Hiermit erkläre ich, dass ich diese Arbeit selbständig verfasst und nur die angegebenen Hilfsmittel benutzt habe.

Oldenburg, den 14.08.2005

.....

Elizabeth von Hauff